Available online at www.sciencedirect.com
ScienceDirect
Journal of Computational Physics 224 (2007) 1095–1123
JOURNAL OF COMPUTATIONAL PHYSICS
www.elsevier.com/locate/jcp

The dynamic procedure for accuracy improvement of numerical discretizations in fluid mechanics

Dieter Fauconnier *, Chris De Langhe, Erik Dick

Department of Flow, Heat and Combustion Mechanics, Ghent University, St. Pietersnieuwstraat 41, B-9000 Ghent, Belgium

Received 27 June 2006; received in revised form 6 November 2006; accepted 7 November 2006
Available online 26 December 2006

Abstract

In CFD computations, discretization or truncation errors should be small providing an acceptable level of accuracy. In this paper, an extension is made of the recently proposed LES formalism based on *sampling operators*. It is shown that the *sampling-based* dynamic procedure, in combination with an appropriate truncation error model, can be used as a technique to increase the numerical accuracy of a discretization. The technique is resemblant to the well-known Richardson extrapolation. The procedure is tested on a 1D convection–diffusion equation and a 2D lid-driven cavity at $Re = 400$, using a finite difference method. Promising results are found.

Keywords: Dynamic procedure; High-order accuracy; Richardson extrapolation

1. Introduction

Numerical discretization errors arise due to the finite representation of the derivative operators on the computational grid. The accuracy of a simulation depends partially on the ability to control these discretization errors. It is known that these errors can be quite large for high wavenumbers, e.g. appearing in steep gradients or small vortices. Especially in large-eddy simulation (LES) of turbulent flows, the smallest resolved scales of the flow still contain a significant amount of energy, and sometimes for low-order discretization schemes, the numerical errors can even become larger than the subgrid term in LES [1–3]. Therefore, discretization errors should be small enough providing an acceptable level of accuracy. Implementing high-order methods or reducing the error by using fine meshes are often computationally prohibitive for CFD simulations in complex geometries. Therefore, there is much interest in improving accuracy while avoiding high computational cost.

Recently, a *new sampling formalism* for large eddy simulation was proposed by Winckelmans et al. [4,5], Debliquy et al. [6] and Knaepen et al. [7]. It is a projection method for Navier–Stokes equations from continuum space to a discrete space, using a sampling operator instead of a filter operator. By thinking in terms of

* Corresponding author. Tel.: +32 9 264 95 21; fax: +32 9 264 35 86.
E-mail address: dieter.fauconnier@ugent.be (D. Fauconnier).

0021-9991/$ - see front matter
doi:10.1016/j.jcp.2006.11.012

such a sampling formalism, the non-linearity in the momentum equations does not result in the generation of subgrid stresses, as the sampling operator commutes with the non-linear terms. However, since the sampling operator is not commutative with spatial derivatives, a closure term appears which represents the loss of information due to the projection on a discrete mesh. In [4–7], a Smagorinsky model was proposed that, by relying on a so-called generalized dynamic procedure uses information from two different grid resolutions, succeeded in accounting for the sampling commutation errors.

This new point of view has led us to further investigate the ability of this sampling-based dynamic procedure, in combination with an appropriate model for the truncation error, to obtain higher-order numerical accuracy. Two possible model families are presented: exact truncation error models and Smagorinsky-like models. The use of generalized dynamic procedure to increase numerical accuracy by comparing solutions on different grid resolutions is reminiscent of the Richardson extrapolation. We show that Richardson extrapolation is a special formulation of the sampling-based generalized dynamic procedure.

The organization of the paper is as follows. First we introduce the sampling formalism in a finite difference context. Then, the generalized dynamic procedure for truncation error modelling is explained and analyzed, and its relation to Richardson extrapolation discussed. We propose two different kinds of models for the truncation error of the Navier–Stokes equations, including two Smagorinsky-like models. Finally, in order to evaluate the numerical qualities of the proposed method, without any turbulence modelling ambiguities, we test the concept on a 1D convection–diffusion equation and a 2D laminar lid-driven cavity at $Re = 400$.

2. The sampling formalism

Consider the continuity equation and the Navier–Stokes equations, for the vector field $\vec{u}(\vec{x},t)$ and the pressure field $p(\vec{x},t)$ of an incompressible fluid ($\rho = 1$) in $\mathbb{R}^n$, $n \in \{1,2,3\}$

$$\frac{\partial u_i}{\partial x_i} = 0 \tag{1}$$

$$\frac{\partial u_i}{\partial t} + u_j \frac{\partial u_i}{\partial x_j} = -\frac{\partial p}{\partial x_i} + \nu \frac{\partial^2 u_i}{\partial x_j^2} \tag{2}$$

Projecting the equations from a continuum physical domain $\Omega \subset \mathbb{R}^n$ to a corresponding discrete physical domain $\Omega^{\Delta_1} = \{\vec{x}_1, \ldots, \vec{x}_N\}$, $\vec{x}_l \in \Omega$ (with N the number of grid points, representing the grid with grid spacing Δ_1), requires the definition of an appropriate projection operator.

Hence, we define the *sampling operator* $\mathscr{S}^{\Delta_1}$, which operates between Ω and Ω^{Δ_1}. This sampling operator $\mathscr{S}^{\Delta_1}$ is idempotent, and commutative with the product of the non-linear terms.

$$\mathscr{S}^{\Delta_1} \circ \mathscr{S}^{\Delta_1} \circ [\phi] = \mathscr{S}^{\Delta_1} \circ [\phi] \tag{3}$$

$$\mathscr{S}^{\Delta_1} \circ [\phi \cdot \psi] = \mathscr{S}^{\Delta_1} \circ [\phi] \cdot \mathscr{S}^{\Delta_1} \circ [\psi] \tag{4}$$

However, $\mathscr{S}^{\Delta_1}$ does not commute with spatial derivatives as they cannot be evaluated at an infinitesimal interval ϵ. For any realistic discrete mesh $\epsilon > 0$ and thus the exact derivative cannot be obtained:

$$\frac{\mathrm{d}\phi}{\mathrm{d}x} \neq \lim_{\Delta \to \epsilon} \frac{\Delta\phi}{\Delta x}$$

When we use the notation $\mathscr{S}^{\Delta_1} \circ u_i = \bar{u}_i$ and $\mathscr{S}^{\Delta_1} \circ \partial = \delta$, applying $\mathscr{S}^{\Delta_1}$ to the continuity equation (1) and the Navier–Stokes equations (2) gives

$$\frac{\delta \bar{u}_i}{\delta x_i} = \Pi^{\Delta_1} \tag{5}$$

$$\frac{\partial \bar{u}_i}{\partial t} + \bar{u}_j \frac{\delta \bar{u}_i}{\delta x_j} = -\frac{\delta \bar{p}}{\delta x_i} + \nu \frac{\delta^2 \bar{u}_i}{\delta x_j^2} + \Sigma_i^{\Delta_1} \tag{6}$$

(7) and (8) are the truncation errors due to the non-commutativity of the operator $\mathscr{S}^{\Delta_1}$ with the spatial derivatives. These truncation terms have the basic form

$$\Pi^{\Delta_1} = \frac{\delta \bar{u}_i}{\delta x_i} - \overline{\frac{\partial u_i}{\partial x_i}} \tag{7}$$

$$\Sigma_i^{\Delta_1} = \bar{u}_j \left(\frac{\delta \bar{u}_i}{\delta x_j} - \overline{\frac{\partial u_i}{\partial x_j}} \right) + \left(\frac{\delta \bar{p}}{\delta x_i} - \overline{\frac{\partial p}{\partial x_i}} \right) - \nu \left(\frac{\delta^2 \bar{u}_i}{\delta x_j^2} - \overline{\frac{\partial^2 u_i}{\partial x_j^2}} \right) \tag{8}$$

Given a discretization scheme for which one can define a sampling operator that satisfies (3) and (4), the exact form for the truncation errors (7) and (8) can be obtained from Taylor series expansion, provided that the field is sufficiently smooth on the grid. We choose the discretization scheme a priori to be second-order central finite difference approximation for both first- and second-order partial derivatives. The grid $\Omega^{\Delta_1} = \{\vec{x}_1, \ldots, \vec{x}_N\}$, $\vec{x}_l \in \Omega$ has a uniform spacing Δx_i in each spatial direction. The finite difference approximations of the derivatives of a scalar u_i with respect to x_j in a node $x_j = x_j^l$ are

$$\frac{\delta \bar{u}_i}{\delta x_j} = \frac{\bar{u}_i(x_j^{l+1}) - \bar{u}_i(x_j^{l-1})}{2\Delta x_j} \tag{9}$$

$$\frac{\delta^2 \bar{u}_i}{\delta x_j^2} = \frac{\bar{u}_i(x_j^{l+1}) - 2\bar{u}_i(x_j^{l}) + \bar{u}_i(x_j^{l-1})}{\Delta x_j^2} \tag{10}$$

Then the Taylor series expansion of the continuous derivative can be written as

$$\overline{\frac{\partial u_i}{\partial x_j}} = \frac{\delta \bar{u}_i}{\delta x_j} - \frac{1}{6}\Delta x_j^2 \overline{\frac{\partial^3 u_i}{\partial x_j^3}} - \frac{1}{120}\Delta x_j^4 \overline{\frac{\partial^5 u_i}{\partial x_j^5}} - \mathcal{O}(\Delta x^6) \tag{11}$$

$$\overline{\frac{\partial^2 u_i}{\partial x_j^2}} = \frac{\delta^2 \bar{u}_i}{\delta x_j^2} - \frac{1}{12}\Delta x_j^2 \overline{\frac{\partial^4 u_i}{\partial x_j^4}} - \frac{1}{360}\Delta x_j^4 \overline{\frac{\partial^6 u_i}{\partial x_j^6}} - \mathcal{O}(\Delta x^6) \tag{12}$$

Substituting the previous expressions in the continuity equation (1) and the Navier–Stokes equations (2) (which is equivalent to applying the sample operator $\mathscr{S}^{\Delta_1}$), leads to the analytical expressions for the truncation terms (7) and (8):

$$\Pi^{\Delta_1} = \frac{1}{6}\Delta x_i^2 \overline{\frac{\partial^3 u_i}{\partial x_i^3}} + \frac{1}{120}\Delta x_i^4 \overline{\frac{\partial^5 u_i}{\partial x_i^5}} + \mathcal{O}(\Delta x^6) \tag{13}$$

$$\begin{aligned} \Sigma_i^{\Delta_1} = {} & \bar{u}_j \left[\frac{1}{6}\Delta x_j^2 \overline{\frac{\partial^3 u_i}{\partial x_j^3}} + \frac{1}{120}\Delta x_j^4 \overline{\frac{\partial^5 u_i}{\partial x_j^5}} + \mathcal{O}(\Delta x^6) \right] \\ & + \left[\frac{1}{6}\Delta x_i^2 \overline{\frac{\partial^3 p}{\partial x_i^3}} + \frac{1}{120}\Delta x_i^4 \overline{\frac{\partial^5 p}{\partial x_i^5}} + \mathcal{O}(\Delta x^6) \right] \\ & - \nu \left[\frac{1}{12}\Delta x_j^2 \overline{\frac{\partial^4 u_i}{\partial x_j^4}} + \frac{1}{360}\Delta x_j^4 \overline{\frac{\partial^6 u_i}{\partial x_j^6}} + \mathcal{O}(\Delta x^6) \right] \end{aligned} \tag{14}$$

Our objective is to obtain a model that increases the accuracy of the second-order approximations, by using information from two different grid resolutions, in the philosophy of the generalized sampling-based dynamic procedure.

3. The generalized dynamic procedure

3.1. Concept

The original dynamic procedure, based on the Germano [8] identity can be extended to a more general approach in the sampling context. Note that Jeanmart and Winckelmans [9] already suggested the use of a sampling operator in the dynamic procedure. The same terminology and notations as in Section (2) are used, which is analogous to the notation of Knaepen et al. [7]. Projection is done of the equations from a continuum

physical domain $\Omega \subset \mathbb{R}^n$ to two corresponding discrete physical domains $\Omega^{\Delta_1} = \{\vec{x}_1, \ldots, \vec{x}_{N_1}\}$, $\vec{x}_l \in \Omega$, and $\Omega^{\Delta_2} = \{\vec{x}_1, \ldots, \vec{x}_{N_2}\}$, $\vec{x}_l \in \Omega$ with $N_2 < N_1$ (in practice, $\Omega^{\Delta_2} \subset \Omega^{\Delta_1}$). This corresponds with the sampling operators $\mathscr{S}^{\Delta_1}$ and $\mathscr{S}^{\Delta_2}$, projecting respectively $\Omega \to \Omega^{\Delta_1}$ and $\Omega \to \Omega^{\Delta_2}$. $\mathscr{S}^{\Delta_2}$ also projects $\Omega^{\Delta_1} \to \Omega^{\Delta_2}$, since

$$\mathscr{S}^{\Delta_2} \circ \mathscr{S}^{\Delta_1} \circ [\phi] = \mathscr{S}^{\Delta_2} \circ [\phi] \tag{15}$$

We keep the notation $\mathscr{S}^{\Delta_1} \circ u_i = \bar{u}_i$ and introduce $\mathscr{S}^{\Delta_2} \circ u_i = \tilde{u}_i = \widetilde{\bar{u}}_i$. We also keep the same notation for the discrete derivative operator $\mathscr{S}^{\Delta_2} \circ \partial = \delta$. Applying the operator $\mathscr{S}^{\Delta_1}$ on the continuity equation (1) and Navier–Stokes equations (2) leads to

$$0 = \mathscr{C}^{\Delta_1}(\bar{u}_i) + \Pi^{\Delta_1} = -\frac{\delta \bar{u}_i}{\delta x_i} + \Pi^{\Delta_1} \tag{16}$$

$$\frac{\partial \bar{u}_i}{\partial t} = \mathscr{N}_i^{\Delta_1}(\bar{u}_i) + \Sigma_i^{\Delta_1} = -\bar{u}_j \frac{\delta \bar{u}_i}{\delta x_j} - \frac{\delta \bar{p}}{\delta x_i} + \nu \frac{\delta^2 \bar{u}_i}{\delta x_j^2} + \Sigma_i^{\Delta_1} \tag{17}$$

We will refer to $\mathscr{C}^{\Delta_1}$ and $\mathscr{N}_i^{\Delta_1}$ as the continuity and Navier–Stokes operators. Similarly, applying $\mathscr{S}^{\Delta_2}$ to the continuous set (1) and (2) gives

$$0 = \mathscr{C}^{\Delta_2}(\tilde{u}_i) + \Pi^{\Delta_2} = -\frac{\delta \tilde{u}_i}{\delta x_i} + \Pi^{\Delta_2} \tag{18}$$

$$\frac{\partial \tilde{u}_i}{\partial t} = \mathscr{N}_i^{\Delta_2}(\tilde{u}_i) + \Sigma_i^{\Delta_2} = -\tilde{u}_j \frac{\delta \tilde{u}_i}{\delta x_j} - \frac{\delta \tilde{p}}{\delta x_i} + \nu \frac{\delta^2 \tilde{u}_i}{\delta x_j^2} + \Sigma_i^{\Delta_2} \tag{19}$$

Ideally, the latter set should also be obtained by applying the sampling operator $\mathscr{S}^{\Delta_2}$ to the first set of equations (16) and (17) giving

$$0 = \mathscr{S}^{\Delta_2} \circ \mathscr{C}^{\Delta_1}(\bar{u}_i) + \mathscr{S}^{\Delta_2} \circ \Pi^{\Delta_1} \tag{20}$$

$$\frac{\partial \tilde{u}_i}{\partial t} = \mathscr{S}^{\Delta_2} \circ \mathscr{N}_i^{\Delta_1}(\bar{u}_i) + \mathscr{S}^{\Delta_2} \circ \Sigma_i^{\Delta_1} \tag{21}$$

Consistency between formulations (18), (19) and (20), (21) imposes the following relations:

$$\mathscr{S}^{\Delta_2} \circ \mathscr{C}^{\Delta_1}(\bar{u}_i) - \mathscr{C}^{\Delta_2}(\tilde{u}_i) = \Pi^{\Delta_2} - \mathscr{S}^{\Delta_2} \circ \Pi^{\Delta_1} \tag{22}$$

$$\mathscr{S}^{\Delta_2} \circ \mathscr{N}_i^{\Delta_1}(\bar{u}_i) - \mathscr{N}_i^{\Delta_2}(\tilde{u}_i) = \Sigma_i^{\Delta_2} - \mathscr{S}^{\Delta_2} \circ \Sigma_i^{\Delta_1} \tag{23}$$

These relations explicitly express the commutation errors made by the projection $\Omega^{\Delta_1} \to \Omega^{\Delta_2}$. The left-hand sides of (22) and (23) are scalar level and vector level equivalents of the Germano identity [8], respectively. They can be determined in terms of the resolved velocity $\bar{u}_i$, since $\mathscr{S}^{\Delta_2} \circ u_i = \tilde{u}_i = \widetilde{\bar{u}}_i$, and play the role of the Leonard scalar (22) or the Leonard vector (23).

We now suppose that models are adopted for both truncation errors Π^{Δ_1} and $\Sigma_i^{\Delta_1}$ which have the basic forms

$$\Pi^{\Delta_1} = C^{\pi} m^{\pi,\Delta_1} \tag{24}$$

$$\Sigma_i^{\Delta_1} = C_i^{\sigma} m_i^{\sigma,\Delta_1} \tag{25}$$

and analogously for the test-level Δ_2. Using a similar terminology as in the classic Germano dynamic procedure [8], the expressions (22) and (23) can then be written as

$$\mathscr{L}^{\pi} = C^{\pi} \mathscr{M}^{\pi} \tag{26}$$

$$\mathscr{L}_i^{\sigma} = C_i^{\sigma} \mathscr{M}_i^{\sigma} \tag{27}$$

in which the Leonard terms $\mathscr{L}$ and the model terms $\mathscr{M}$ read

$$\mathscr{L}^{\pi} = \mathscr{S}^{\Delta_2} \circ \mathscr{C}^{\Delta_1}(\bar{u}_i) - \mathscr{C}^{\Delta_2}(\tilde{u}_i) \tag{28}$$

$$\mathscr{L}_i^{\sigma} = \mathscr{S}^{\Delta_2} \circ \mathscr{N}_i^{\Delta_1}(\bar{u}_i) - \mathscr{N}_i^{\Delta_2}(\tilde{u}_i) \tag{29}$$

$$\mathscr{M}^{\pi} = m^{\pi,\Delta_2} - \mathscr{S}^{\Delta_2} \circ m^{\pi,\Delta_1} \tag{30}$$

$$\mathscr{M}_i^{\sigma} = m_i^{\sigma,\Delta_2} - \mathscr{S}^{\Delta_2} \circ m_i^{\sigma,\Delta_1} \tag{31}$$

The Leonard terms are thus resemblant to the expressions (7) and (8). Explicitly, they are written as

$$\mathscr{L}^{\pi} = \widetilde{\frac{\delta \bar{u}_i}{\delta x_i}} - \frac{\delta \widetilde{\bar{u}}_i}{\delta x_i} \tag{32}$$

$$\mathscr{L}_i^{\sigma} = \widetilde{\bar{u}}_j \left(\widetilde{\frac{\delta \bar{u}_i}{\delta x_j}} - \frac{\delta \widetilde{\bar{u}}_i}{\delta x_j} \right) + \left(\widetilde{\frac{\delta \bar{p}}{\delta x_i}} - \frac{\delta \widetilde{\bar{p}}}{\delta x_i} \right) - \nu \left(\widetilde{\frac{\delta^2 \bar{u}_i}{\delta x_j^2}} - \frac{\delta^2 \widetilde{\bar{u}}_i}{\delta x_j^2} \right) \tag{33}$$

Similar expressions are obtained for the model terms. In the approach of e.g. Knaepen et al. [7], a single field C^{σ} was used to model the error of the separate momentum equations, leading to a least-square optimization procedure as a compromise between the three independent conditions (27). Here we propose separate fields C_i^{σ} for the separate equations, for which the optimal parameter can be determined from every independent condition (27).

For the computations presented in this paper, it was often necessary to filter the quantities before calculating the scalar fields C^{π} and C_i^{σ}, to remove undesirable high frequency pollution or singularities, leading to instability of the solution. We use the least-square method

$$C^{\pi} = \frac{\langle \mathscr{L}^{\pi} \mathscr{M}^{\pi} \rangle}{\langle \mathscr{M}^{\pi} \mathscr{M}^{\pi} \rangle} \tag{34}$$

$$C_i^{\sigma} = \frac{\langle \mathscr{L}_i^{\sigma} \mathscr{M}_i^{\sigma} \rangle}{\langle \mathscr{M}_i^{\sigma} \mathscr{M}_i^{\sigma} \rangle} \tag{35}$$

in which $\langle \cdot \rangle$ denotes a smoothing filter, such as a local moving average or a global average. For the latter averaging, constant fields are obtained. C^{π} and C_i^{σ} can be positive or negative, depending on the adopted discretization scheme. Therefore, it was sometimes necessary to apply clipping to avoid excessive negative values of C^{π} and C_i^{σ} causing instability of the solution. Finally, C^{π} and C_i^{σ}, which are calculated on the coarse grid, are interpolated to the fine grid using a piecewise cubic Hermite interpolation. A fully embedded test grid is applied.

3.2. Relationship to Richardson extrapolation

We use the notation $\left.\frac{\delta^n u}{\delta x^n}\right|^{\Delta}$ for the finite difference approximation of the nth-order derivative on a grid with grid spacing Δ. Consider the Taylor series expansion of the nth-order derivative, $n = 0, 1, 2, \ldots$, for a kth-order central discretization scheme ($k = 2, 4, 6, \ldots$)

$$\frac{\partial^n u}{\partial x^n}(x) = \left.\frac{\delta^n \bar{u}}{\delta x^n}\right|^{\Delta} + c_k \Delta^k \frac{\partial^{k+n} u}{\partial x^{k+n}} + \mathscr{O}(\Delta^{k+2}) \tag{36}$$

$$\frac{\partial^n u}{\partial x^n}(x) = \left.\frac{\delta^n \tilde{u}}{\delta x^n}\right|^{2\Delta} + c_k (2\Delta)^k \frac{\partial^{k+n} u}{\partial x^{k+n}} + \mathscr{O}(\Delta^{k+2}) \tag{37}$$

in which the coefficients c_k are grid independent. We now assume that the leading order truncation term is an adequate model for the complete truncation error. Discretization of this term and applying the generalized dynamic procedure, without averaging, leads to a coefficient c_k

$$c_k = \frac{\left.\frac{\delta^n \tilde{u}}{\delta x^n}\right|^{2\Delta} - \left.\frac{\delta^n \bar{u}}{\delta x^n}\right|^{\Delta}}{\Delta^k \left.\frac{\delta^{k+n} \bar{u}}{\delta x^{k+n}}\right|^{\Delta} - (2\Delta)^k \left.\frac{\delta^{k+n} \tilde{u}}{\delta x^{k+n}}\right|^{2\Delta}} \tag{38}$$

substitution of which in (36) finally results in

$$\frac{\partial^n u}{\partial x^n}(x) \approx \frac{2^k \left.\frac{\delta^n \bar{u}}{\delta x^n}\right|^{\Delta} \left.\frac{\delta^{k+n} \tilde{u}}{\delta x^{k+n}}\right|^{2\Delta} - \left.\frac{\delta^n \tilde{u}}{\delta x^n}\right|^{2\Delta} \left.\frac{\delta^{k+n} \bar{u}}{\delta x^{k+n}}\right|^{\Delta}}{2^k \left.\frac{\delta^{k+n} \tilde{u}}{\delta x^{k+n}}\right|^{2\Delta} - \left.\frac{\delta^{k+n} \bar{u}}{\delta x^{k+n}}\right|^{\Delta}} \tag{39}$$

This non-linear expression is closely related to Richardson extrapolation. Under the assumption

$$\left.\frac{\delta^{k+n}\tilde{u}}{\delta x^{k+n}}\right|^{2\Delta} \equiv \left.\frac{\delta^{k+n}\bar{u}}{\delta x^{k+n}}\right|^{\Delta} \equiv \frac{\partial^{k+n}u}{\partial x^{k+n}} \tag{40}$$

the general formula for Richardson extrapolation is obtained

$$\frac{\partial^n u}{\partial x^n}(x) \approx \frac{2^k \left.\frac{\delta^n \bar{u}}{\delta x^n}\right|^{\Delta} - \left.\frac{\delta^n \tilde{u}}{\delta x^n}\right|^{2\Delta}}{2^k - 1} + \mathcal{O}(\Delta^{k+2}) \tag{41}$$

which is fully equivalent with a $(k+2)$th-order accurate central scheme for the nth derivative. We will call expression (41) the *implicit or differential Richardson extrapolation*.

Although (41) is the general expression, Richardson extrapolation is more familiar for $n = 0$

$$u(x) \approx \frac{2^k \bar{u}|^{\Delta} - \tilde{u}|^{2\Delta}}{2^k - 1} + \mathcal{O}(\Delta^{k+2}) \tag{42}$$

In this *explicit or classical* form, the Richardson extrapolation method needs the solution to be computed on two different grids, which is demanding in computational effort. In the *differential* form, the field $u(x)$ does not necessarily have to be computed twice, as the coarse grid can be obtained from sampling the fine-grid field. This allows to obtain higher-order discretizations for derivatives. For example, the fourth-order central finite difference scheme can be constructed from the second-order central scheme on two different grids.

Traditionally, the *classical* Richardson extrapolation is the most common one. It is used as a post-processor to two solutions on two different grids with no reference to the codes, algorithms or governing equations that produced the solutions [10]. The *differential* Richardson extrapolation is rather rare. However, a similar approach is used in a finite volume context by Verstappen et al. [11,12]. The momentum equations are then physically integrated over both the original control volumes of the mesh and three times larger control volumes corresponding to a three times coarser mesh.

A major drawback of the *classical* Richardson extrapolation is that it does not preserve conservation. This is due to the more fundamental problem that the extrapolated values are no longer internally consistent, since they do not satisfy a system of finite difference approximations [13]. However, this can be remedied by using the differential form or the dynamic procedure, as they are part of the system of finite difference equations.

3.3. Single-wave Fourier analysis

For further analysis of expression (39), and the implications of approximation (40), we would like to perform a Fourier analysis on the kth-order accurate nth-order derivative. Because expression (39) is non-linear, it should be linearized first in order to perform a Fourier analysis which is valid for an arbitrary field containing a spectrum of wavenumbers. However, for reasons of simplicity we first consider a single-wave Fourier analysis of the non-linear expression although we emphasize that the conclusions cannot be extrapolated straightforwardly to a more general arbitrary field as superposition cannot be applied to a non-linear expression. However, in the next section, we will perform a multiple-wave analysis.

We adopt Taylor series expansion on both the fine and the coarse grid, and we introduce a blending factor f in order to switch between the dynamic procedure (39) ($f = 1$) and Richardson extrapolation (41) ($f = 0$), and to investigate intermediate behaviour:

$$\frac{\partial^n u}{\partial x^n}(x) = \left.\frac{\delta^n \bar{u}}{\delta x^n}\right|^{\Delta} + c_k \Delta^k \left.\frac{\delta^{k+n}\bar{u}}{\delta x^{k+n}}\right|^{\Delta} \tag{43}$$

$$\frac{\partial^n u}{\partial x^n}(x) = \left.\frac{\delta^n \tilde{u}}{\delta x^n}\right|^{2\Delta} + c_k (2\Delta)^k \left(f \left.\frac{\delta^{k+n}\tilde{u}}{\delta x^{k+n}}\right|^{2\Delta} + (1-f) \left.\frac{\delta^{k+n}\bar{u}}{\delta x^{k+n}}\right|^{\Delta} \right) \tag{44}$$

for which the dynamic procedure results in

$$c_k = \frac{\left|\frac{\delta^n \bar{u}}{\delta x^n}\right|^{\Delta} - \left|\frac{\delta^n \tilde{u}}{\delta x^n}\right|^{2\Delta}}{(1-2^k)\Delta^k \left|\frac{\delta^{k+n} \bar{u}}{\delta x^{k+n}}\right|^{\Delta} - 2^k \Delta^k f \left(\left|\frac{\delta^{k+n} \bar{u}}{\delta x^{k+n}}\right|^{2\Delta} - \left|\frac{\delta^{k+n} \tilde{u}}{\delta x^{k+n}}\right|^{\Delta}\right)} \tag{45}$$

The resulting coefficient can only be meaningfull for values of f within the range $[0,1]$, however it can be easily verified that for arbitrary large values of f, (49) reduces to kth-order accuracy as $\lim_{f\to\infty} c_k = 0$. From Richardson extrapolation we learn that the denominator of (45) is proportional to the $(k+n)$th-order derivative, or

$$\left|\frac{\delta^n \bar{u}}{\delta x^n}\right|^{\Delta} - \left|\frac{\delta^n \tilde{u}}{\delta x^n}\right|^{2\Delta} = c_k^*(1-2^k)\Delta^k \left|\frac{\delta^{k+n} \bar{u}}{\delta x^{k+n}}\right|^{\Delta} \tag{46}$$

in which c_k^* is then a known constant from the Taylor series expansion. Substitution into expression (45) and rearranging results in

$$c_k = c_k^* \frac{1}{1 - \frac{2^k f}{(1-2^k)} \left(\frac{\left|\frac{\delta^{k+n} \bar{u}}{\delta x^{k+n}}\right|^{2\Delta} - \left|\frac{\delta^{k+n} \bar{u}}{\delta x^{k+n}}\right|^{\Delta}}{\left|\frac{\delta^{k+n} \bar{u}}{\delta x^{k+n}}\right|^{\Delta}} \right)} \tag{47}$$

$$c_k \approx c_k^* \frac{1}{1 - \mathcal{O}(\Delta^k)} \tag{48}$$

This clearly shows that the non-linearity which appears in the final expression is rather weak as it is of order $\mathcal{O}(\Delta^k)$. Because of this, it can be expected that a single-wave Fourier analysis should give some representative results.

Substitution of expression (49) into the fine-grid Taylor series (43) leads to the final expression

$$\frac{\partial^n u}{\partial x^n}(x) = \left|\frac{\delta^n \bar{u}}{\delta x^n}\right|^{\Delta} + \frac{c_k^*}{1 - \frac{2^k f}{(1-2^k)} \left(\frac{\left|\frac{\delta^{k+n} \bar{u}}{\delta x^{k+n}}\right|^{2\Delta} - \left|\frac{\delta^{k+n} \bar{u}}{\delta x^{k+n}}\right|^{\Delta}}{\left|\frac{\delta^{k+n} \bar{u}}{\delta x^{k+n}}\right|^{\Delta}} \right)} \Delta^k \left|\frac{\delta^{k+n} \bar{u}}{\delta x^{k+n}}\right|^{\Delta} \tag{49}$$

In Fourier space, the nth derivative can be written as

$$\mathscr{F}\left(\frac{\delta^n \bar{u}}{\delta x^n}\right) = (\mathrm{i}\kappa')^n \mathscr{F}(\bar{u}) \tag{50}$$

with κ' the modified wavenumber. The modified wavenumber represents here the amplitude error of the discrete derivatives for a single wave with relative wavenumber $\frac{\kappa}{\kappa_{\max}}$. Modified wavenumbers and the corresponding absolute errors of $\frac{\delta u}{\delta x}$ and $\frac{\delta^2 u}{\delta x^2}$ are given in Figs. 1 and 2 for a second-, fourth-, sixth-, eighth- and 10th-order central scheme, and also for the expression (49). The latter is given at values of $f = 1, \frac{1}{2}, \frac{1}{3}, \frac{1}{4}, \frac{1}{5}, \frac{1}{10}$. Since, an exact fourth-order scheme is obtained with the differential Richardson extrapolation ($f = 0$), their modified wavenumbers are equal. The full dynamic procedure with $f = 1$ leads to a singularity for approximately $\frac{\kappa}{\kappa_{\max}} \approx 0.38$, as the denominator in expression (49) becomes zero (Fig. 1b). However, by decreasing the blending factor, the spectral behaviour improves significantly for both $\frac{\delta u}{\delta x}$ and $\frac{\delta^2 u}{\delta x^2}$. It can be seen from both graphs, that an optimum can be obtained within the range $f \in [\frac{1}{3}, \frac{1}{5}]$. Closer inspection of the error given in the logarithmic graph, shows that for $f = \frac{1}{5}$, the overall accuracy of the dynamic procedure is close to sixth order. Fig. 1d shows that for the lower part of the wavenumber space, the accuracy is then sixth order, whereas at higher wavenumbers the accuracy drops to approximately fifth order. Increasing the blending factor to e.g., $f = \frac{1}{4}$ or even $f = \frac{1}{3}$ gives better accuracy for high wavenumbers but at the cost of the low wavenumbers, which still obtain at least fourth order. This may be interesting for large-eddy simulation, where the smallest scales could be resolved more accurately, whereas the largest scales still reach more than fourth-order accuracy. However, in laminar flows, where the highest wavenumber is supposed to be a few times smaller than the grid-cutoff, a blending factor $f = \frac{1}{5}$ should be advantageous.

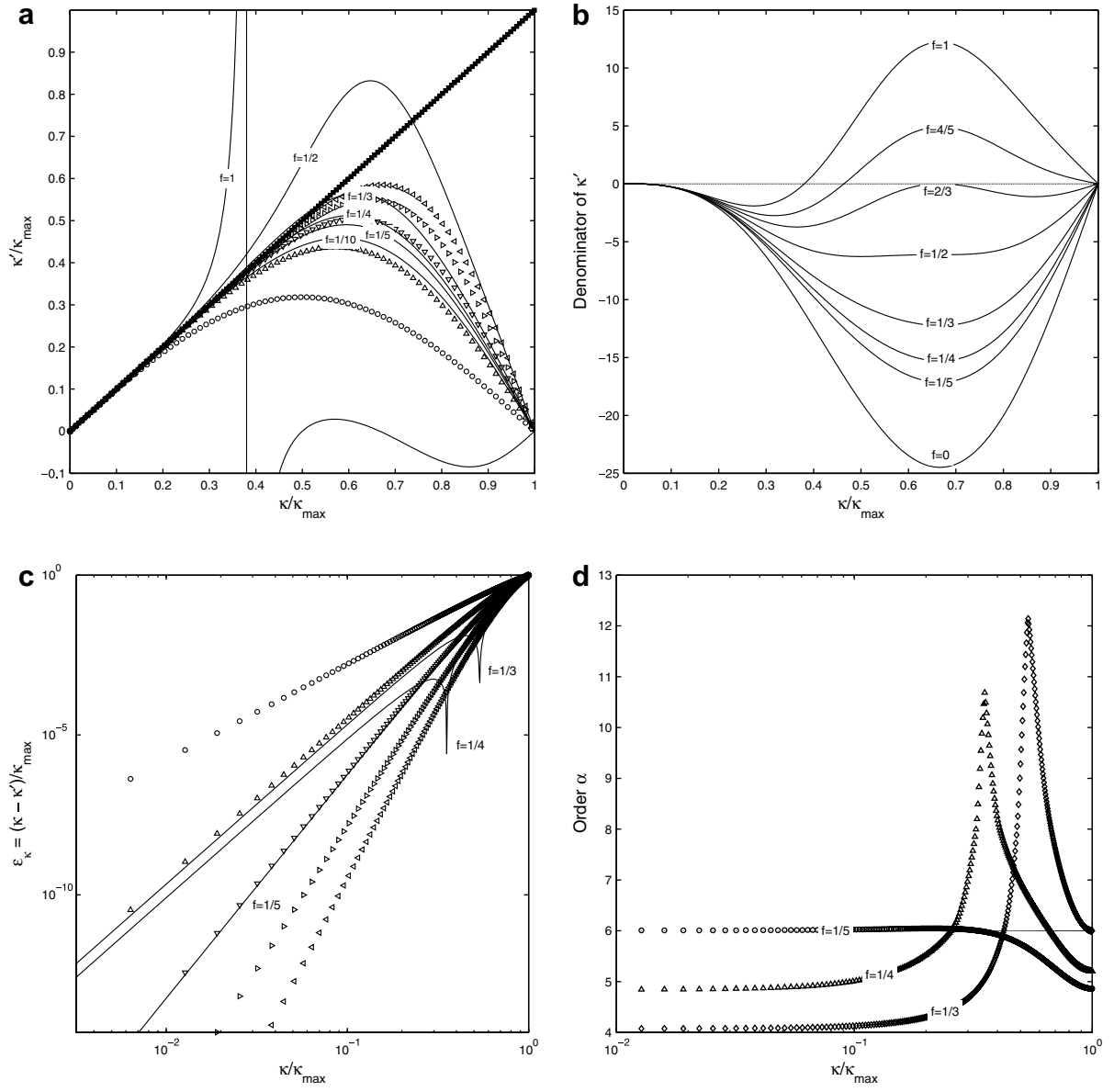

Fig. 1. Single-wave analysis for $\frac{\partial u}{\partial x}$: (a) Modified wavenumbers and (c) absolute error ε_κ: (■) spectral; (○) second-order central; (△) fourth-order central; (▽) sixth-order central; (▷) eighth-order central; (◁) 10th-order central; (—) dynamic procedure. (b) Denominator of the modified wavenumber for varying f. (d) Accuracy-order α in $\mathcal{O}(\Delta^\alpha)$.

Again, we emphasize that the observations based on a single wave cannot be extended straightforwardly to the analysis fo the non-linear scheme. Nevertheless, we still expect them to be more or less indicative for a more arbitrary field containing multiple wavenumbers. This will be confirmed in the following paragraph.

3.4. Multiple-wave Fourier analysis

To investigate further the role of the weak non-linearity in the expressions above, a Fourier analysis considering multiple waves is necessary. Here, we restrict ourself to a double-wave analysis. Consider the double-wave scalar field

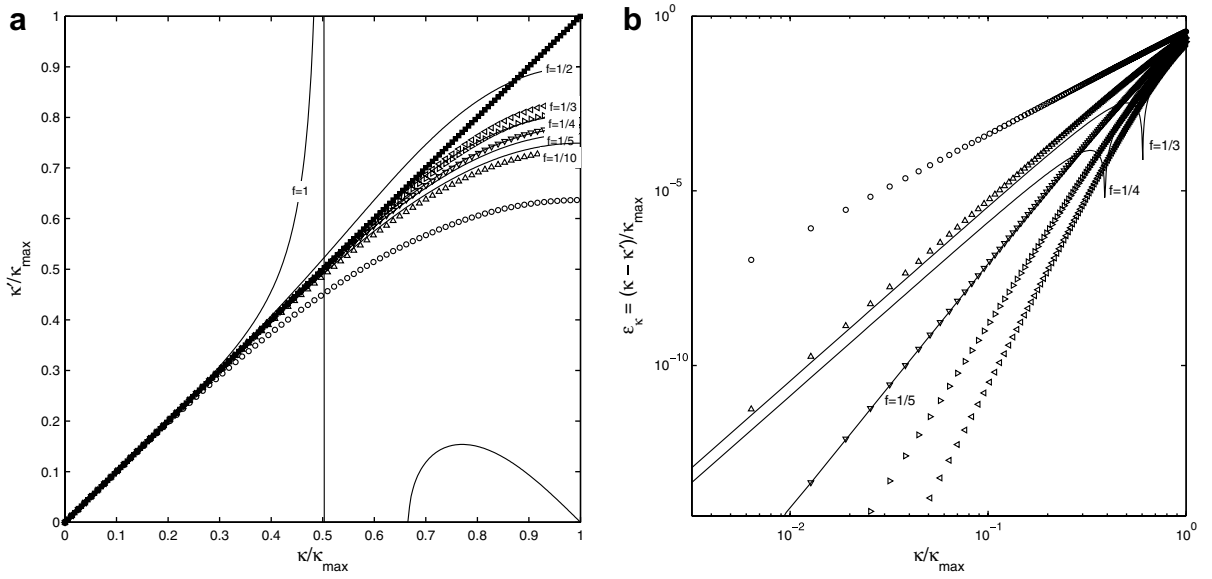

Fig. 2. Single-wave analysis for $\frac{\partial^2 u}{\partial x^2}$: (a) Modified wavenumbers and (b) absolute error ε_κ: (■) spectral; (○) second-order central; (△) fourth-order central; (▽) sixth-order central; (▷) eighth-order central; (◁) 10th-order central; (—) dynamic procedure.

$$u(\kappa,\mu,x) = \mathrm{e}^{(\mathrm{i}\kappa x)} + \mathrm{e}^{(\mathrm{i}\mu x)} \tag{51}$$

for which the analytic expression of the gradient is

$$\frac{\partial^n u}{\partial x^n}(\kappa,\mu,x) = (\mathrm{i}\kappa)^n \mathrm{e}^{(\mathrm{i}\kappa x)} + (\mathrm{i}\mu)^n \mathrm{e}^{(\mathrm{i}\mu x)} \tag{52}$$

Although a modified wavenumber cannot longer be defined in this approach, it is still possible to obtain a transfer function of the resulting schemes. The transfer function at random position $x = x_i$ is defined as

$$\mathscr{G}(\kappa,\mu) = \frac{\left|\frac{\delta^n \tilde{u}}{\delta x^n}(\kappa,\mu,x_i)\right|}{\left|\frac{\partial^n u}{\partial x^n}(\kappa,\mu,x_i)\right|} \tag{53}$$

Fig. 3 shows the transfer functions for the second- and sixth-order schemes and also for the dynamic procedure with blending factors $f = 1$ and $f = \frac{1}{5}$. It can be noticed that the full dynamic procedure has a similar behaviour like in the single-wave analysis, as it leads again to singularities for certain combinations of the wavenumbers κ and μ. However, decreasing the blending factor to values within the range $f \in \left[\frac{1}{5},\frac{1}{3}\right]$ improves the performance of the dynamic procedure. Because the interpretation of the transfer functions in Fig. 3 is rather difficult, an order estimation is done to measure the performance of the dynamic procedure at the values $f = \left[\frac{1}{3},\frac{1}{4},\frac{1}{5}\right]$. Results are presented in Fig. 4. It can be seen that the conclusions drawn in the single-wave analysis hold for the double-wave analysis. For $f = \frac{1}{5}$ the dynamic procedure reaches sixth-order accuracy for the lower part of the wavenumber space, whereas at higher wavenumbers the accuracy drops to approximately fifth order. For $f = \frac{1}{4}$ or even $f = \frac{1}{3}$ better accuracy for high wavenumbers can be obtained but at the cost of the low wavenumbers, which still obtain at least fourth order. Considering the fact that we will only simulate laminar flows, we are now able to propose a blending factor $f = \frac{1}{5}$ for further study, such that the accuracy order is as high as possible for the lower wavenumber part.

3.5. Grid-convergence

The investigation of the dynamic procedure in Fourier space lead us to conclude that one can obtain higher-order accuracy by using a dynamic scheme (49), with an appropriate value of the blending factor f. In view of

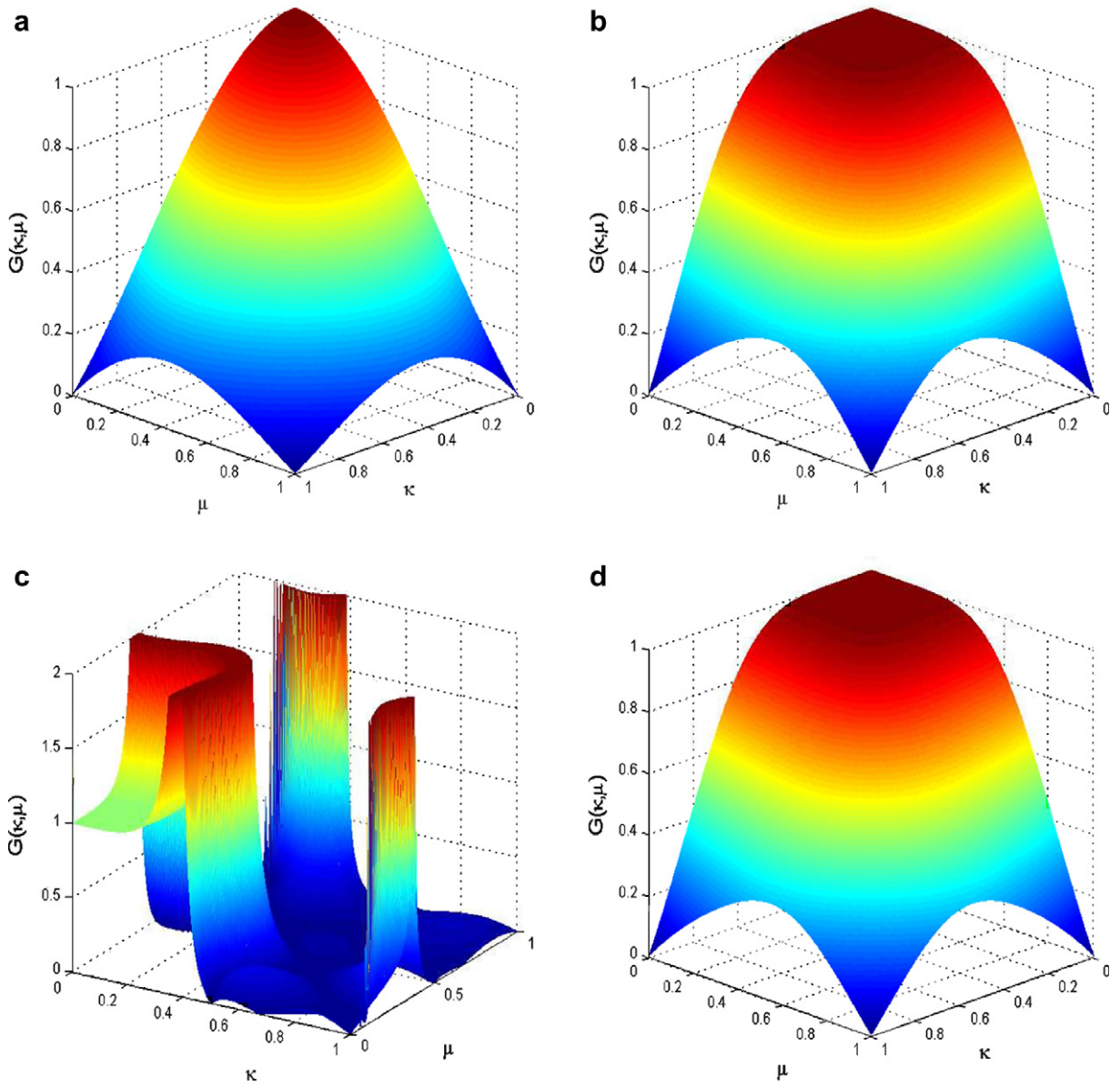

Fig. 3. Multiple-wave analysis for $\frac{\partial u}{\partial x}$: (a) $\mathscr{G}(\kappa,\mu)$ for a second-order scheme; (b) $\mathscr{G}(\kappa,\mu)$ for a sixth-order scheme; (c) $\mathscr{G}(\kappa,\mu)$ for the dynamic procedure ($f=1$); (d) $\mathscr{G}(\kappa,\mu)$ for the dynamic procedure ($f=\frac{1}{5}$).

the applications presented in this work, we have chosen $f=\frac{1}{5}$ in order to optimise the accuracy at the lower wavenumber range of the spectrum. In this paragraph we will focus on the behaviour of the dynamic procedure (with $f=\frac{1}{5}$) in physical space. More specifically we will conduct a grid-refinement study of the dynamic procedure applied on the discrete gradient.

Consider the periodic function

$$u(x)=\sin(x)+\sin(2x)+\sin(4x) \tag{54}$$

defined in the periodic domain $x=[0,2\pi]$. Since, the analytical derivative $\frac{\partial u}{\partial x}$ is known, we can define three standard norms to represent the discretization error of the discrete derivative on a grid with n nodes and grid spacing Δ

$$L_1 = \frac{1}{n} \left| \left(\left(\frac{\delta \bar{u}}{\delta x}\right)_{x=x_k} \right| \tag{55}$$

$$L_2 = \sqrt{\frac{n}{=1} \left(- \left(\frac{\delta \bar{u}}{\delta x}\right)_{x=x_k} \right)^2} \tag{56}$$

$$L_\infty = \mathrm{n} \left(\left(\frac{\delta \bar{u}}{\delta x}\right)_{x=x_k} \right| \tag{57}$$

The L_1-norm ıre mean absolute error in the domain, the L_2-norm is related to the standard deviation σ of th oı $L_1^2 + \sigma^2$, and finally the L_∞ gives the maximum value of the absolute error in the domain. The rc re presented for six different implementations of the dynamic procedure in Fig. 5 as function e ing $\Delta = \frac{2\pi}{n-1}$ while refining the grid from $n = 2^4$ to $n = 2^9$. In the left column in Fig. 5, c_k ha eı d in every fine-grid point, while in the right column c_k has been evaluated at the coarse g :v 5a and b we calculated the dynamic coefficient as $c_k = \frac{L}{M}$, while in Fig. 5e and f, a constant fic ɔbtained through a least-square approximation $c_k = \frac{\langle LM \rangle}{\langle MM \rangle}$. For the two remaining Fig. 5c and i te approach was followed by calculating the dynamic coefficient as a three point moving aver $_k$ It can be seen from Fig. 5a that the dynamic procedure with the pointwise evaluation of the fi ery fine-grid point indeed obtains sixth-order accuracy for all norms, although we notice a wea tt $_\infty$ for the lower grid resolutions. Pointwise coarse grid evaluation of the dynamic constant lea s tering of L_∞, as well as for L_1 and L_2. Closer investigation learns that the main trend for the o ıs sixth order, while for the L_2-norm fifth-order accuracy is obtained. For the L_∞-norm only f d be reached. From the implementation using a least-square approximation for the constant fi difference can be distinguished between the fine-grid or coarse grid evaluation of the dynaı ɔ e see that this rather rough approximation leads for both evaluations to a loss in order: the e to fifth order for coarse grids, but for the finer grids, the curves deflect to fourth order. This s ror norms. The observed deflection most likely finds its cause in the weak nonlinearity of ı ficient, which is of order $\mathcal{O}(\Delta^k)$, and thus gets more important when decreasing the grid resc ı ɛless, we notice from the Fig. 5e and f that, although the order is lost, the error levels produ y ɛdure are still smaller than those of the fourth-order scheme. Similar results are seen when u h average approach presented in Fig. 5c and d. The main trend for the L_1-norm is almost six c for the L_2-norm approximately fifth-order accuracy is obtained. The L_∞-norm reaches agai ccuracy. Like in the least-square approach, we notice a deflection of the curves as they tend ɔ slopes for coarser grids. Moreover, the overall error level is again lower than that of the fourth ı Γo conlcude this paragraph, the dynamic procedure seems to be an optimization procedure th ɛ nize the local truncation error. For any simplification or restriction made to the

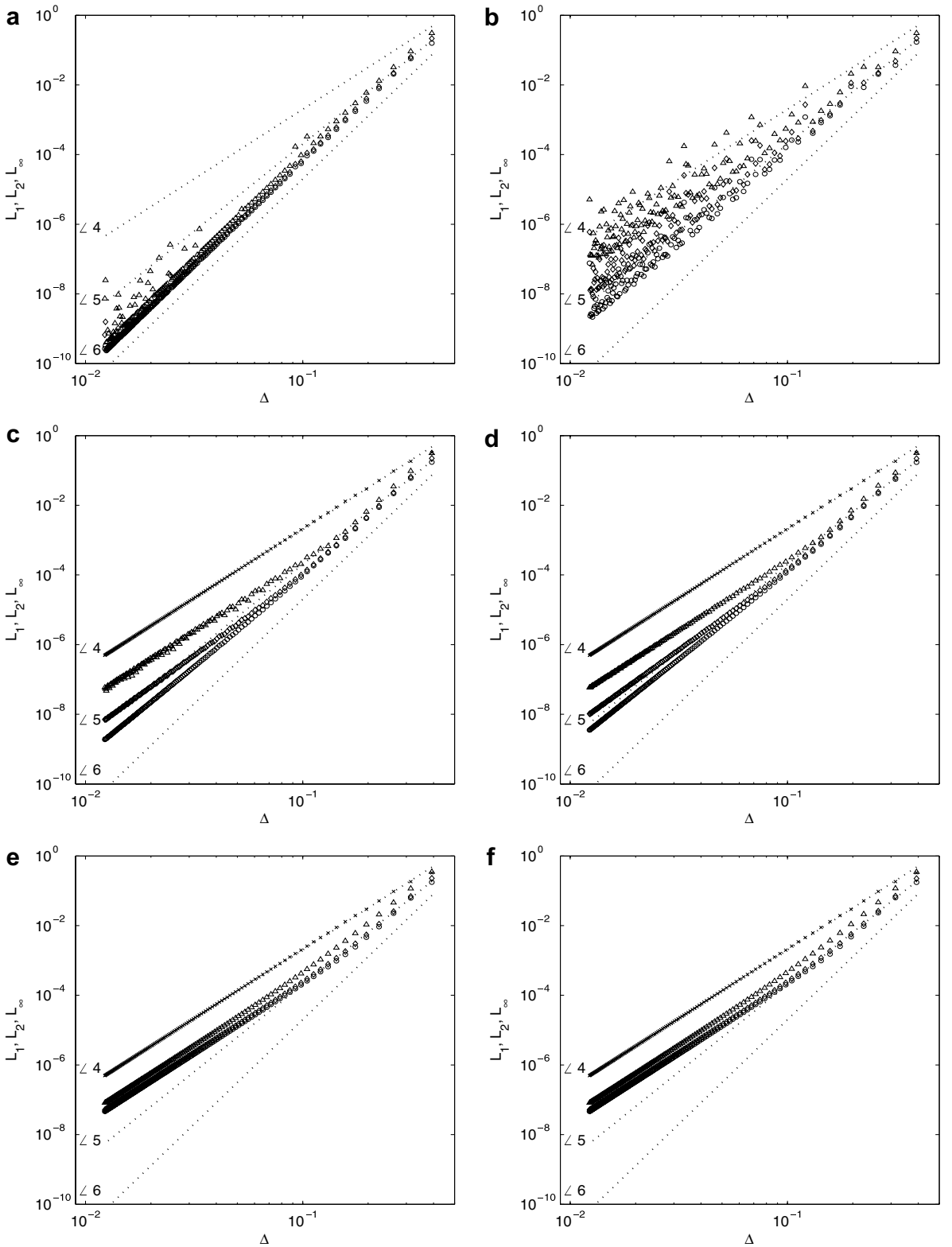

Fig. 5. Error norms L_1 (○), L_2 (◇) and L_∞ (△) of $\frac{\partial u}{\partial x}$: (a) Pointwise c_k on Δ; (b) Pointwise c_k on 2Δ; (c) Moving average c_k on Δ; (d) Moving average c_k on 2Δ; (e) least-square c_k on Δ; (f) least-square c_k on 2Δ. (. . .) represent slopes 4, 5 and 6 and (×) is L_1-norm of a fourth-order finite difference scheme.

Table 1
Overhead percentages of the different schemes

Second (%)	Fourth (%)	Sixth (%)	Eighth (%)	Tenth (%)	DP (%)
0	1.73	3.45	5.11	6.68	26.05
−3.34	−1.67	0	1.60	3.12	21.85

First row normalised to second-order scheme; second row normalised to sixth-order scheme.

calculation of the dynamic coefficient (least-square, moving average), there is a price to pay in terms of quality, but although the order reduces, the overall error is still minimized.

3.6. Computational cost

Comparing the computational cost of the dynamic procedure with a traditional finite difference method is rather complicated as it highly depends on the efficiency of the implementation and on the programming environment. Therefore it may be more useful to adopt a more basic point of view by looking at the number of (additional) operations. It can be understood from equation (47) that the evaluation of the higher-order term $\mathcal{O}(\Delta^k)$ in the dynamic coefficient, which clearly ensures the higher-order behaviour of the procedure, will be responsible for an additional cost of the dynamic procedure. How severe that cost is, mainly depends on the implementation of c_k. It is obvious that calculation of c_k on the coarse grid followed by a simple interpolation to the fine grid, takes less computational time in comparison with a full evaluation of c_k on the fine grid. However, if c_k is calculated using a least-square method or a moving average method, the computational cost will not only be determined by some extra arithmetic operations, but, mainly by the implementation efficiency of these techniques. This makes it difficult to accurately predict the computational cost. For these same reasons, we decided to restrict ourself to a simple numerical experiment in which only the cost of the dynamic procedure with the pointwise evaluation of c_k on the fine grid was compared to the cost of the traditional finite difference schemes. In this way, no ambiguities arise due to interpolations or averaging techniques, but only the cost of additional arithmetic operations is accounted for. In the experiment the computational time was measured for the evaluation of the gradient with different schemes. However, it should be noticed that a high-level programming language was used with low-level efficiency. The overhead compared to the second-order scheme and to the sixth-order scheme is displayed in Table 1. The pure dynamic procedure seems to have an 22% additional cost compared to the sixth-order scheme, independent of the value of the blending factor. From a theoretical point of view, evaluating c_k on the coarse grid is expected to be much less expensive as only half of the operations is needed. It may be worthwhile to mention that although the procedure has an additional cost on a single grid evaluation, the additional cost in a multigrid environment is quasi nil, as solutions on several grid levels are then fully available. In this case, extrapolation methods in general are very attractive.

4. Modelling the truncation error of the Navier–Stokes equations

4.1. Exact truncation error model

Instead of evaluating a truncation correction for every separate derivative in the Navier–Stokes equations, which is straightforward, we would like to know if we could increase the accuracy of the discretization by using one model for all truncation errors together, like in the philosophy of [7]. Argueing that the leading terms of the Taylor series expansion are the most important (being the largest source of error), we take them as the basic modelling ingredients, and rewrite (13) and (14) as

$$\Pi^{\Delta_1} = \left(\frac{1}{6} + \frac{1}{120}\Delta x_i^2 \frac{\overline{\partial^5 u_i}}{\partial x_i^5}\left(\frac{\overline{\partial^3 u_i}}{\partial x_i^3}\right)^{-1} + \dots\right)\Delta x_i^2 \frac{\overline{\partial^3 u_i}}{\partial x_i^3} \tag{58}$$

$$\Sigma_i^{\Delta_1} = \bar{u}_j \left(\frac{1}{6} + \frac{1}{120} \Delta x_j^2 \frac{\overline{\partial^5 u_i}}{\partial x_j^5} \left(\frac{\overline{\partial^3 u_i}}{\partial x_j^3} \right)^{-1} + \ldots \right) \Delta x_j^2 \frac{\overline{\partial^3 u_i}}{\partial x_j^3} + \left(\frac{1}{6} + \frac{1}{120} \Delta x_i^2 \frac{\overline{\partial^5 p}}{\partial x_i^5} \left(\frac{\overline{\partial^3 p}}{\partial x_i^3} \right)^{-1} + \ldots \right) \Delta x_i^2 \frac{\overline{\partial^3 p}}{\partial x_i^3} - \frac{v}{2} \left(\frac{1}{6} + \frac{1}{180} \Delta x_j^2 \frac{\overline{\partial^6 u_i}}{\partial x_j^6} \left(\frac{\overline{\partial^4 u_i}}{\partial x_j^4} \right)^{-1} + \ldots \right) \Delta x_j^2 \frac{\overline{\partial^4 u_i}}{\partial x_j^4} \tag{59}$$

We now make the assumption that to a certain degree of accuracy we can merge the different series between the brackets in (59) into the *vector* field C_i^σ. Similarly denoting the terms between brackets in (58) by the *scalar* field C^π, we obtain as modelling basis

$$\Pi^{\Delta_1} = C^\pi \Delta x_i^2 \frac{\delta^3 \bar{u}_i}{\delta x_i^3} \tag{60}$$

$$\Sigma_i^{\Delta_1} = C_i^\sigma \left(\bar{u}_j \Delta x_j^2 \frac{\delta^3 \bar{u}_i}{\delta x_j^3} + \Delta x_i^2 \frac{\delta^3 \bar{p}}{\delta x_i^3} - \frac{v}{2} \Delta x_j^2 \frac{\delta^4 \bar{u}_i}{\delta x_j^4} \right) \tag{61}$$

For a 2D flow, this results in

$$\Pi^{\Delta_1} = C^\pi \left\{ \Delta x^2 \frac{\delta^3 \bar{u}}{\delta x^3} + \Delta y^2 \frac{\delta^3 \bar{v}}{\delta y^3} \right\} \tag{62}$$

$$\Sigma_u^{\Delta_1} = C_u^\sigma \left\{ \Delta x^2 \left(\bar{u} \frac{\delta^3 \bar{u}}{\delta x^3} + \frac{\delta^3 \bar{p}}{\delta x^3} - \frac{v}{2} \frac{\delta^4 \bar{u}}{\delta x^4} \right) + \Delta y^2 \left(\bar{v} \frac{\delta^3 \bar{u}}{\delta y^3} - \frac{v}{2} \frac{\delta^4 \bar{u}}{\delta y^4} \right) \right\} \tag{63}$$

$$\Sigma_v^{\Delta_1} = C_v^\sigma \left\{ \Delta x^2 \left(\bar{u} \frac{\delta^3 \bar{v}}{\delta x^3} - \frac{v}{2} \frac{\delta^4 \bar{v}}{\delta x^4} \right) + \Delta y^2 \left(\bar{v} \frac{\delta^3 \bar{v}}{\delta y^3} + \frac{\delta^3 \bar{p}}{\delta y^3} - \frac{v}{2} \frac{\delta^4 \bar{v}}{\delta y^4} \right) \right\} \tag{64}$$

This model in which C_i^σ and C^π are obtained dynamically, is closely related to the exact expression of the truncation error for a second-order accurate discretization, and therefore we call it the *exact truncation model*. Adopting values $C^\pi = \frac{1}{6}$ and $C_i^\sigma = \frac{1}{6}$ one obtains a fourth-order accurate discretization. The major drawback of the model is the requirement of a broader 5-point stencil to evaluate the third- and fourth-order derivatives. This can be very unpleasant near walls, where even excentric 6-point stencils (also second-order accurate) have to be constructed to maintain the overall accuracy. It would be more convenient if the higher-order derivatives could be reduced to maximum second order, the highest appearing order in the physical Navier–Stokes equations.

4.2. Smagorinksy-like models

The idea behind the reduction of the high-order derivatives for modelling purposes, is based on the observation that the Taylor series of the finite difference approximation of an odd order derivative contains only odd higher-order derivatives, whereas the Taylor series of an even order derivative contains only even higher-order derivatives. More specificly, higher-order derivatives appearing in the analytical Taylor series of a central finite difference approximation of the derivative display a similar behaviour as the derivative itself, although they do not have the same scaling. In short, all odd (respectively even) order derivatives behave more or less similarly. Here we propose to approximate the higher-order derivatives by an appropriate non-linear combination of lower-order ones, taking the above observations into consideration. Therefore we adopt the following modelling approximation (no summation):

$$\bar{u}_i \frac{\delta^n \bar{u}_i}{\delta x_j^n} \approx \left(\frac{\delta^p \bar{u}_i}{\delta x_j^p} \right) \left(\frac{\delta^q \bar{u}_i}{\delta x_j^q} \right) \tag{65}$$

in which $(p + q) = n$. If n is even, p and q should both be even. If n is odd, then p should be even and q should be odd, or vice versa. This reduction can be applied repeatedly, such that actually every high-order derivative may be reduced to a combination of first and second-order derivatives, properly rescaled with $\bar{u}_i$.

If $n = 3$, and if we choose $p = 1$, $q = 2$, a Smagorinsky-like approximation appears. The convective terms in (59) will be modelled through (65) as

$$\bar{u}_j \frac{\delta^3 \bar{u}_i}{\delta x_j^3} \approx \frac{\bar{u}_j}{\bar{u}_i} \frac{\delta \bar{u}_i}{\delta x_j} \frac{\delta^2 \bar{u}_i}{\delta x_j^2} \tag{66}$$

The disadvantage of this model is that a division by $\bar{u}_i$ appears, which will inevitably lead to singularities, as $\bar{u}_i$ can be zero. Therefore, we propose the following Smagorinsky-like model for the convective terms

$$\Sigma_{i,\mathrm{conv}}^{\Delta_1} = C_i^{\sigma*} \Delta x_j^2 u_j \frac{\delta \bar{u}_i}{\delta x_j} \frac{\delta^2 \bar{u}_i}{\delta x_j^2} \tag{67}$$

in which the dimensional field $C_i^{\sigma*} = \frac{C_i^{\sigma}}{\bar{u}_i}$ is calculated dynamically.

Further approximations can be made by assuming that $\frac{\bar{u}_j}{\bar{u}_i} \approx 1$, and by taking the absolute value of the first-order derivative. One then obtains an expression very close to the classic Smagorinsky subgrid model

$$\bar{u}_j \frac{\delta^3 \bar{u}_i}{\delta x_j^3} \approx \left| \frac{\delta \bar{u}_i}{\delta x_j} \right| \frac{\delta^2 \bar{u}_i}{\delta x_j^2} \tag{68}$$

leading to a second model for the convective terms in a Smagorinsky-like way

$$\Sigma_{i,\mathrm{conv}}^{\Delta_1} = C_i^{\sigma} \Delta x_j^2 \left| \frac{\delta \bar{u}_i}{\delta x_j} \right| \frac{\delta^2 \bar{u}_i}{\delta x_j^2} \tag{69}$$

in which the dimensionless field C_i^{σ} is calculated dynamically. In both Smagorinsky-like models an additional approximation is made by giving all approximated terms in the model the same coefficient.

For the truncation error of the continuity equation (58) and the pressure terms and the viscous terms in the momentum equations, the modelling hypothesis (65) does not lead directly to a suitable Smagorinsky-like model. Therefore, we decide to either leave the exact truncation error models in their original forms for these terms, or to neglect them completely. The latter may be justified for the pressure and viscous terms in the momentum equations as we expect the convective terms to be dominant. There is less justification for neglecting the truncation error in the continuity equation. This hypothesis will be verified in the test cases.

For a 2D flow the first Smagorinsky-like model is

$$\Pi^{\Delta_1} = C^{\pi} \left\{ \Delta x^2 \frac{\delta^3 \bar{u}}{\delta x^3} + \Delta y^2 \frac{\delta^3 \bar{v}}{\delta y^3} \right\} \tag{70}$$

$$\Sigma_u^{\Delta_1} = C_{u,1}^{\sigma*} \left\{ \Delta x^2 u \frac{\delta \bar{u}}{\delta x} \frac{\delta^2 \bar{u}}{\delta x^2} + \Delta y^2 v \frac{\delta \bar{u}}{\delta y} \frac{\delta^2 \bar{u}}{\delta y^2} \right\} + C_{u,2}^{\sigma} \left\{ \Delta x^2 \left(\frac{\delta^3 \bar{p}}{\delta x^3} - \frac{\nu}{2} \frac{\delta^4 \bar{u}}{\delta x^4} \right) - \Delta y^2 \frac{\nu}{2} \frac{\delta^4 \bar{u}}{\delta y^4} \right\} \tag{71}$$

$$\Sigma_v^{\Delta_1} = C_{v,1}^{\sigma*} \left\{ \Delta x^2 u \frac{\delta \bar{v}}{\delta x} \frac{\delta^2 \bar{v}}{\delta x^2} + \Delta y^2 v \frac{\delta \bar{v}}{\delta y} \frac{\delta^2 \bar{v}}{\delta y^2} \right\} + C_{v,2}^{\sigma} \left\{ -\Delta x^2 \frac{\nu}{2} \frac{\delta^4 \bar{v}}{\delta x^4} + \Delta y^2 \left(\frac{\delta^3 \bar{p}}{\delta y^3} - \frac{\nu}{2} \frac{\delta^4 \bar{v}}{\delta y^4} \right) \right\} \tag{72}$$

and the second Smagorinsky-like model is

$$\Pi^{\Delta_1} = C^{\pi} \left\{ \Delta x^2 \frac{\delta^3 \bar{u}}{\delta x^3} + \Delta y^2 \frac{\delta^3 \bar{v}}{\delta y^3} \right\} \tag{73}$$

$$\Sigma_u^{\Delta_1} = C_{u,1}^{\sigma} \left\{ \Delta x^2 \left| \frac{\delta \bar{u}}{\delta x} \right| \frac{\delta^2 \bar{u}}{\delta x^2} + \Delta y^2 \left| \frac{\delta \bar{u}}{\delta y} \right| \frac{\delta^2 \bar{u}}{\delta y^2} \right\} + C_{u,2}^{\sigma} \left\{ \Delta x^2 \left(\frac{\delta^3 \bar{p}}{\delta x^3} - \frac{\nu}{2} \frac{\delta^4 \bar{u}}{\delta x^4} \right) - \Delta y^2 \frac{\nu}{2} \frac{\delta^4 \bar{u}}{\delta y^4} \right\} \tag{74}$$

$$\Sigma_v^{\Delta_1} = C_{v,1}^{\sigma} \left\{ \Delta x^2 \left| \frac{\delta \bar{v}}{\delta x} \right| \frac{\delta^2 \bar{v}}{\delta x^2} + \Delta y^2 \left| \frac{\delta \bar{v}}{\delta y} \right| \frac{\delta^2 \bar{v}}{\delta y^2} \right\} + C_{v,2}^{\sigma} \left\{ -\Delta x^2 \frac{\nu}{2} \frac{\delta^4 \bar{v}}{\delta x^4} + \Delta y^2 \left(\frac{\delta^3 \bar{p}}{\delta y^3} - \frac{\nu}{2} \frac{\delta^4 \bar{v}}{\delta y^4} \right) \right\} \tag{75}$$

5. Simulations and results

In order to evaluate the numerical qualities of the dynamic procedure, in the absence of possible interactions caused by turbulence modelling aspects, we choose to test it on a laminar flow. We first analyse the

method on a 1D convection–diffusion equation. Then we study the more complex flow of a 2D-driven cavity at Reynolds number $Re = 400$. We use intentionally a uniform grid to avoid any ambiguity toward the dynamic procedure.

5.1. 1D convection–diffusion equation

5.1.1. Case setup

The continuum convection–diffusion equation defined in the physical domain $\Omega = [0, L] \subset \mathbb{R}$, supplemented by a set of Dirichlet boundary conditions, reads

$$\begin{aligned} &\frac{\partial u}{\partial x} = \frac{v}{c}\frac{\partial^2 u}{\partial x^2} \\ &u(0) = u_0 \\ &u(L) = u_L \end{aligned} \tag{76}$$

Here c is the convective speed and v the viscosity. Defining the Péclet number $Pe = \frac{L}{\kappa}$, with $\kappa = \frac{v}{c}$ (Pe is the one-dimensional equivalent of the Reynolds number), the analytic solution of the convection–diffusion equation reads

$$u(x) = u_0 + (u_L - u_0)\frac{1 - e^{\frac{x}{\kappa}}}{1 - e^{Pe}} \tag{77}$$

and is displayed in Fig. 6.

Projecting the continuum equation (76) from Ω to the uniformly spaced grid $\Omega^{\Delta_1} = \{x_1 = 0, \ldots, x_N = L\}$, with $x_I \in \Omega$ and grid spacing Δx, leads to the discretized equation

$$\begin{aligned} &\frac{\delta \bar{u}}{\delta x} = \kappa \frac{\delta^2 \bar{u}}{\delta x^2} + \Sigma^{\Delta_1} \\ &\bar{u}(x_1) = u_0 \\ &\bar{u}(x_N) = u_L \end{aligned} \tag{78}$$

with Σ^{Δ_1} the truncation error depending on the discretization scheme. We propose for Σ^{Δ_1} the basic form

$$\Sigma^{\Delta_1} = \kappa_I \frac{\delta^n \bar{u}}{\delta x^n} \tag{79}$$

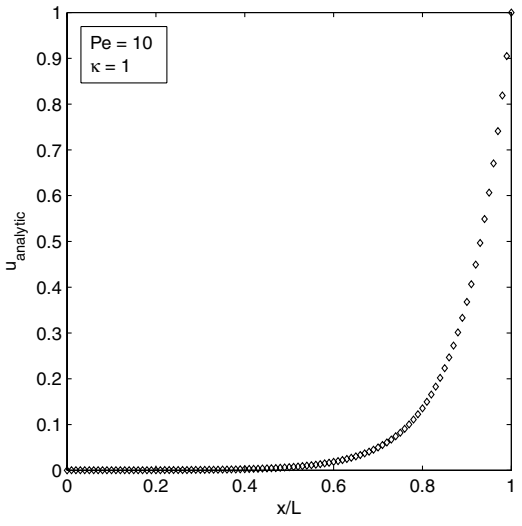

Fig. 6. Analytic solution ($N = 51$) for the 1D convection–diffusion equation with $Pe = 10$ and $\kappa = 1$ in the domain $\Omega^{\Delta_1} = [0, 10]$.

Table 2
Overview of the different simulations of the convection diffusion equation for a second-order central discretization

Code	$\Sigma_i^{\Delta_1}$	κ_t	n
cd.a	$\frac{1}{6}\Delta x^2\frac{\partial^3 u}{\partial x^3}-\frac{\kappa}{12}\Delta x^2\frac{\partial^4 u}{\partial x^4}$	$C^\sigma\Delta x^2$	3
cd.b	$\frac{1}{6}\Delta x^2\frac{\partial^3 u}{\partial x^3}-\frac{\kappa}{12}\Delta x^2\frac{\partial^4 u}{\partial x^4}$	$C^\sigma\frac{\Delta x^2}{\kappa}$	2
cd.c	$\frac{1}{6}\Delta x^2\frac{\partial^3 u}{\partial x^3}-\frac{\kappa}{12}\Delta x^2\frac{\partial^4 u}{\partial x^4}$	$C^\sigma\Delta x$	2
cd.d	$\frac{1}{6}\Delta x^2\frac{\partial^3 u}{\partial x^3}-\frac{\kappa}{12}\Delta x^2\frac{\partial^4 u}{\partial x^4}$	$C^\sigma\frac{\Delta x^2}{c}\lvert\frac{\delta\tilde{u}}{\delta x}\rvert$	2

An overview of the tested models for a second-order central discretization of both the convective and diffusive terms is given in Table 2. Models cd.a and cd.b are related to the exact truncation error model. Note that for $C^\sigma=\frac{1}{12}$ an exact fourth-order accuracy is reached for model cd.a. Because of the relation

$$\frac{\partial u}{\partial x}=\kappa\frac{\partial^2 u}{\partial x^2}=\kappa^2\frac{\partial^3 u}{\partial x^3}=\kappa^3\frac{\partial^4 u}{\partial x^4}=\ldots \tag{80}$$

models cd.a and cd.b are analytically fully equivalent:

$$\Sigma^{\Delta_1}=\frac{1}{6}\Delta x^2\frac{\partial^3 u}{\partial x^3}-\frac{\kappa}{12}\Delta x^2\frac{\partial^4 u}{\partial x^4} \tag{81}$$

$$=\frac{1}{6}\Delta x^2\frac{\partial^3 u}{\partial x^3}-\frac{1}{12}\Delta x^2\frac{\partial^3 u}{\partial x^3} \tag{82}$$

$$=\frac{1}{12}\frac{\Delta x^2}{\kappa}\frac{\partial^2 u}{\partial x^2} \tag{83}$$

This artifact is only present in this simple linear problem. It allows us to investigate the effects of broader stencils and their evaluation at the wall. Inconsistencies appear when evaluating the stencils at different grids (Ω^{Δ_1} and Ω^{Δ_2}) in near wall nodes, because of the use of excentric stencil formulations respecting the general order of accuracy. This is shown schematically in Fig. 7, where the 3rd derivative evaluated at the coarse grid near wall node has different stencils on the coarse and the fine grids. As a consequence, an incorrect value for C^σ is generated in the first coarse grid node near the wall and the wall node itself if $n\geqslant 3$. Therefore these values cannot be used for interpolation to the fine grid. In order to avoid these anomalies we extrapolate $\mathscr{L}$ and $\mathscr{M}$ in the affected points. A piecewise cubic Hermite extrapolation is used. We like to emphasize that we intentionally include the inconsistent model cd.c, with incorrect order of accuracy, and the Smagorinsky-like model cd.d, which does not correspond completely to the hypothesis (65), in order to investigate the robustness of the method. In this test case, no least-square averaging method was used to calculate C^σ. Thus, $C^\sigma=\frac{L}{M}$.

5.1.2. Results and discussion

Simulations are performed on a uniform mesh with 50 cells and 100 cells. The adopted parameters are $c=0.1$, $\nu=0.1$, $L=10$ so that $Pe=10$. We define the pointwise error in the domain as

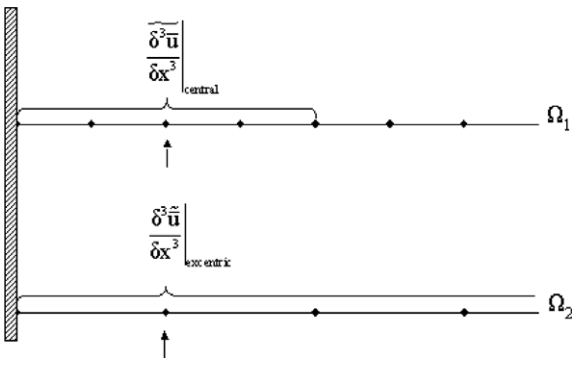

Fig. 7. Inconsistency of the procedure near walls.

$$\varepsilon_u(x) = |u(x) - u_{\text{analytic}}(x)| \tag{84}$$

Furthermore, we investigate the order of accuracy through the previously defined error norms L_1, L_2 and L_∞ obtained from a grid-refinement study using the model cd.a. The results presented in Figs. 8 and 9 are within the expectations for this simple linear problem.

It can be seen from both graphs that the dynamic procedure with the quasi-theoretical model cd.a and $f = \frac{1}{5}$ obtains much higher accuracy than the fourth-order solution, however, it does not display a consistent higher-order convergence in the grid spacing. The order of convergence for the error norms L_1, L_2 and L_∞ displays a deflection from fourth to sixth order when going from fine to coarse grids especially with a blending factor $f = \frac{1}{4}$. Moreover, it can be seen that although the proposed optimal blending factor $f = \frac{1}{5}$ gives a significant accuracy improvement compared to the fourth-order solution, a blending factor of $f = \frac{1}{4}$ leads to even better

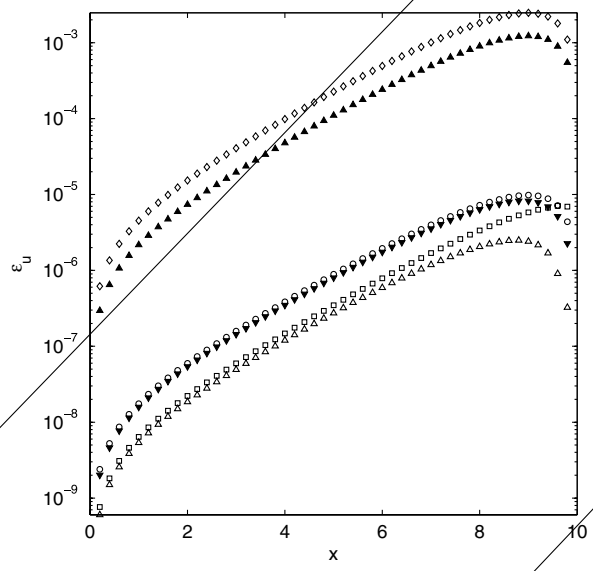

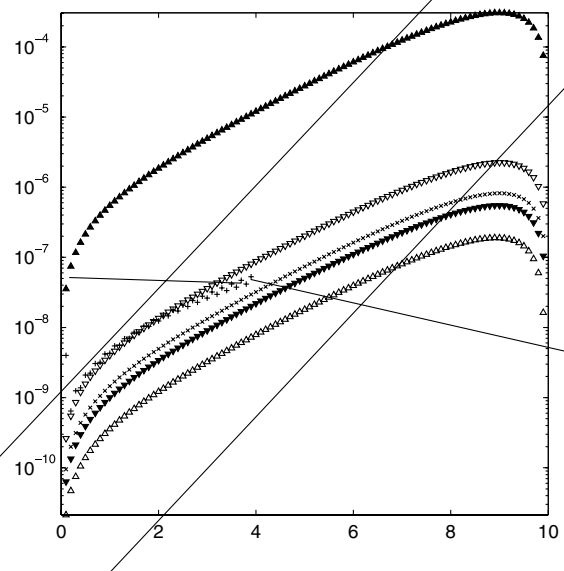

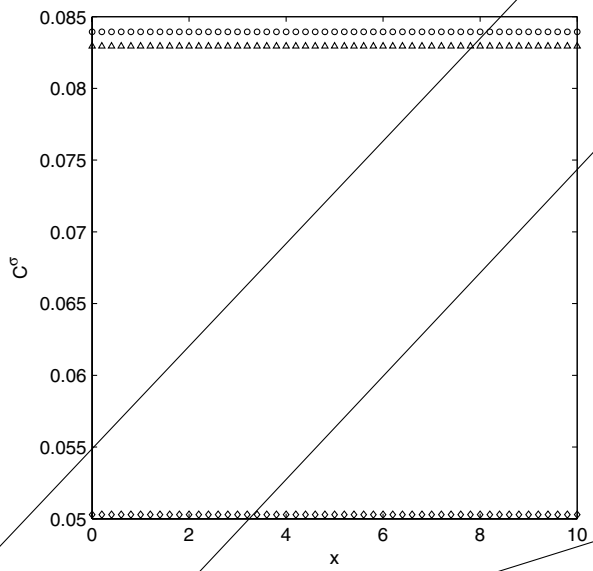

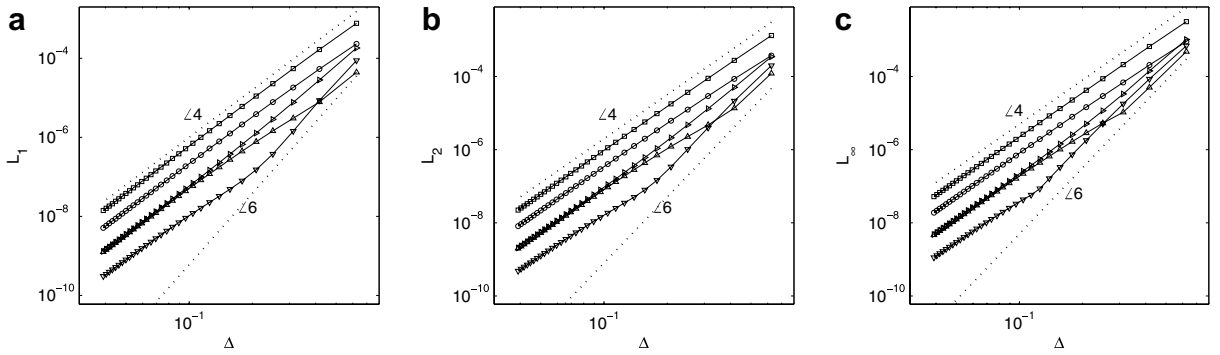

Fig. 9. Grid-refinement study for model cd.a: (a) L_1-norm; (b) L_2-norm; (c) L_∞-norm. (○) fourth-order solution ($f=0$); (□) $f=1$; (△) $f=\frac{1}{5}$; (▽) $f=\frac{1}{4}$; (▷) $f=\frac{1}{3}$; (...) slopes of order 4 and 6.

results in this case. Nevertheless, we believe that this coincidence cannot be generalized. The reason for the deflection of the convergence-slopes is twofold. On the one hand we transformed the current model cd.a using the analytical equation into a reduced form, while on the other hand we assumed one dynamic coefficient for the complete truncation error. Most likely the second assumption is the most dominant because the optimized dynamic coefficient of the first derivative is not necessarily the same as the optimized dynamic coefficient of the second derivative in the equation. This means that for the finer grids, the misfit between both virtual coefficients is more severe while for the coarser grids, the optimization procedure succeeds in finding a minimal common higher-order term $\mathcal{O}(\Delta^k)$ in the dynamic coefficient for the complete truncation term. This also means that the influence of the higher-order term $\mathcal{O}(\Delta^k)$ in this coefficient is increasingly important with Δ such that a sixth-order slope is reached. Further, the differential Richardson extrapolation ($f=0$) obtains fourth-order accuracy approximately. The classical Richardson extrapolation, combining two resolved solutions on two different grids, seems to be less accurate than the fourth-order solution, and displays a very irregular behaviour. The analytically reduced model cd.b reaches only fourth-order accuracy, although it is equivalent to cd.a. This can be explained by the fact that the stencils used in cd.b are smaller than those of cd.a. Further it can be seen from the poor results of model cd.c that the leading order in the grid spacing should be respected. The Smagorinsky-hypothesis (65) seems to be justified as the results of model cd.d clearly show. Only some small loss of accuracy with respect to model cd.a is observed. Finally if $f=1$, rather poor results are obtained with model cd.a, as could be expected from the spectral analysis. It can be seen that the value of C^σ for the models cd.a and cd.b are constant and close to the theoretical value $C^\sigma=\frac{1}{12}$. However, for the Smagorinsky-like model cd.d, C^σ does not remain constant, but shows an exponential-like behaviour. We divided the Smagorinsky-like model by the constant convective speed c to obtain the dimensionless parameter C^σ. This is however not justified in the philosophy of the modelling hypothesis (65), as we should have divided it by the transported quantity $\bar{u}$ itself. Consequently, C^σ compensates for $\frac{1}{\bar{u}}$, which explains the displayed behaviour.

5.2. 2D lid-driven cavity

5.2.1. Case setup

In the driven cavity, an internal recirculating flow is generated by a uniform moving wall in a 2D square closed domain (Fig. 10). The flow is representative for more complex situations with vortices and secondary flows, and is a challenging test case. On each wall, impermeability conditions and no-slip conditions are imposed. This implies that the fluid is supposed to move with the lid at the lid, and that it is stationary at the two side walls and the bottom wall. This leads to so-called corner singularities at both top corners due to the discontinuity in the imposed boundary conditions.

A pseudo-compressible code is used with a third-order Runge–Kutta method for stepping in pseudo-time. Spatial discretization is second-order central for all terms. The pressure field is extrapolated at the wall using the fourth-order accurate Neumann condition $\frac{\partial^3 p}{\partial n^3}=0$ with n the wall-normal direction, and the mean value is

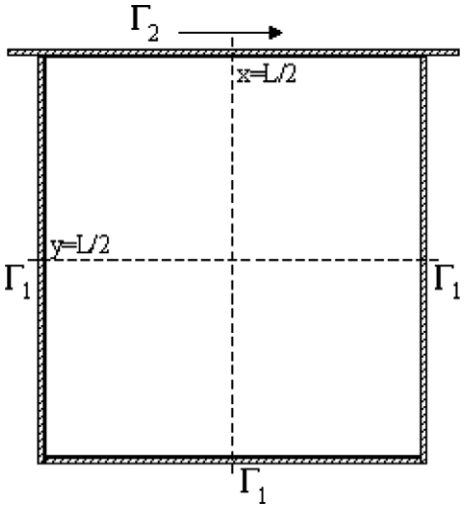

Fig. 10. Geometry of the square lid-driven cavity.

kept at zero. The Reynolds number, based on the height and lid-velocity is $Re = 400$, for which the flow is laminar. The governing equations in the physical domain $\Omega = [0, L] \times [0, L] \subset \mathbb{R}^2$, read:

$$\frac{1}{\beta^2}\frac{\partial p}{\partial t} + \frac{\partial u_i}{\partial x_i} = 0 \tag{85}$$

$$\frac{\partial u_i}{\partial t} + u_j\frac{\partial u_i}{\partial x_j} = -\frac{\partial p}{\partial x_i} + \nu\frac{\partial^2 u_i}{\partial x_j^2} \tag{86}$$

with β the artificial speed of sound. The Dirichlet boundary conditions are $u_i = 0$ on Γ_1 en $u_i = u_{lid}$ on Γ_2. Projecting the continuum equations from Ω to the discrete mesh $\Omega^{\Delta_1} = \{x_1 = 0, \ldots, x_{N_x} = L\} \times \{y_1 = 0, \ldots, y_{N_y} = L\}$, with $\{x_l, y_l\} \in \Omega$ and uniform grid spacings Δx and Δy, leads to the discretized equations

$$\frac{1}{\beta^2}\frac{\delta \bar{p}}{\delta t} + \frac{\delta \bar{u}_i}{\delta x_i} = \Pi^{\Delta_1} \tag{87}$$

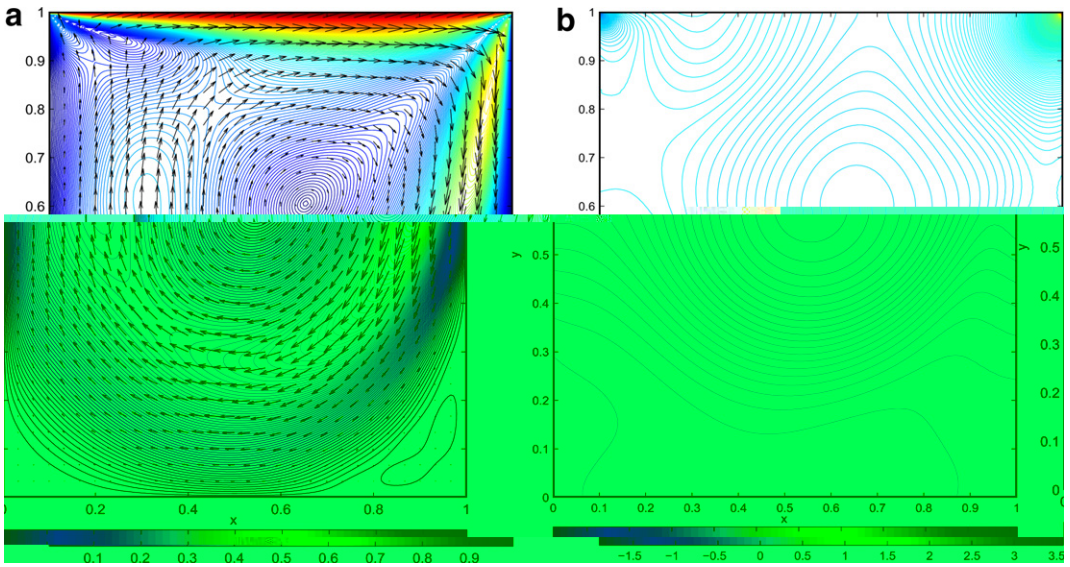

Fig. 11. Sixth-order reference solution on a 180×180 grid: (a) vector field and contours of velocity magnitude; (b) contours of pressure field.

$$\frac{\delta \bar{u}_i}{\delta t} + \bar{u}_j \frac{\delta \bar{u}_i}{\delta x_j} = -\frac{\delta \bar{p}}{\delta x_i} + \nu \frac{\delta^2 \bar{u}_i}{\delta x_j^2} + \Sigma_i^{\Delta_1} \tag{88}$$

Although an artificial dissipation is generally required in the continuity equation to damp the wiggles generated by the central scheme, no dissipation has been implemented here, in order to avoid possible interference with the dynamic model. Therefore, the fields contain a minimal spurious pressure mode that however does not affect the velocity results. The exact truncation errors are given in previous paragraphs. As no analytical solution is available, we use a sixth-order central scheme on a 180×180 mesh, to generate the reference solution. The flow pattern of the reference solution is given in Fig. 11. Cross-section profiles of the reference solution and a second-order solution on a 60×60 mesh are shown in Fig. 12. It can be noticed that both solutions are very close to each other. For this test case, the error for a variable ϕ is defined as

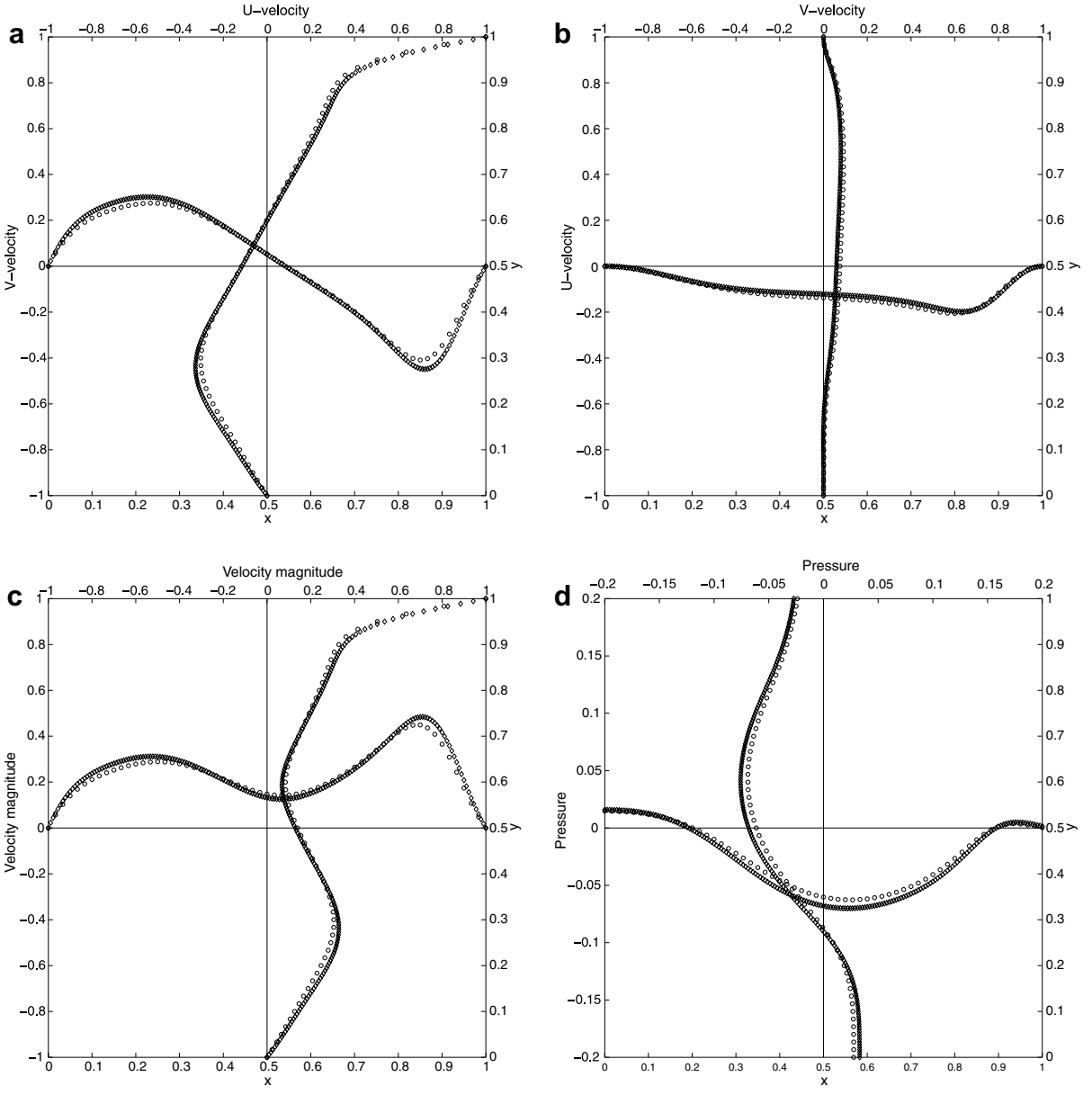

Fig. 12. Cross-section profiles (◇) sixth-order reference solution on a 180×180 grid; (○) second-order solution on a 60×60 grid.

Table 3
Overview of the different simulations in the square lid-driven cavity

Code	Continuity	Momentum	
		Convective	Pressure and viscous
$ldc.2o_{60\times60}$	Second-order central	Second-order central	
$ldc.4o_{60\times60}$	Fourth-order central	Fourth-order central	
$ldc.6o_{60\times60}$	Sixth-order central	Sixth-order central	
$ldc.1a_{60\times60}$	Exact $+ f = \frac{1}{5}$	Exact $+ f = \frac{1}{5}$	
$ldc.1b_{60\times60}$	Exact $+ f = 1$	Exact $+ f = 1$	
$ldc.1c_{60\times60}$	None	Exact $+ f = \frac{1}{5}$	
$ldc.2a_{60\times60}$	Exact	Exact + conv. Leonard	None
$ldc.2b_{60\times60}$	Exact	Exact + full Leonard	None
$ldc.3a_{60\times60}$	Exact	Smagorinsky 1	Exact
$ldc.3b_{60\times60}$	Exact	Smagorinsky 1	Fourth order
$ldc.3c_{60\times60}$	Exact	Smagorinsky 1	None
$ldc.3d_{60\times60}$	Exact	Smagorinsky 2	None

$$\varepsilon_\phi = \phi_{\text{reference}} - \phi_{\text{resolved}} \tag{89}$$

The different simulations are given in Table 3. Using the exact truncation error model in combination with the dynamic procedure, a global least-square averaging over the whole field was chosen for C^π and C^σ. This is justified because of the uniform grid and because the basic behaviour of C^π and C^σ is expected to be approximately uniform (close to the theoretical value of $\frac{1}{6}$). For the Smagorinsky-like models however, we use a local least-square averaging over a 3×3 subdomain. For the first Smagorinsky-like model a clipping to $C^\sigma > -0.2$, to prevent excessive negative values of C^σ, was necessary. For the second Smagorinsky-like model a clipping to $C^\sigma > -0.16$ was necessary. For all models, including the Smagorinsky models, a blending factor $f = \frac{1}{5}$ as in formula (49) was used, unless stated otherwise.

5.2.2. Results and discussion

The results for the cross-sections $x = \frac{L}{2}$ and $y = \frac{L}{2}$, which are given in Figs. 13–16, correspond to the general expectations. First, it can be seen from Fig. 13 that the classical Richardson extrapolation ($ldc.RE_{60\times60}$) does not reach the accuracy of the fourth-order solution, unlike the differential form ($ldc.DRE_{60\times60}$), which obtains approximately fourth order. This indicates that the classical Richardson extrapolation does not seem to be very reliable compared to its equivalent differential form. Probably this has to do with the fact that the differential form satisfies the set of differential equations unlike its classical counterpart. As expected, the dynamic procedure, with the exact truncation model ($ldc.1a_{60\times60}$) and the optimal blending factor of $\frac{1}{5}$ lies very close to the sixth-order solution, as shown in Fig. 14. In contrast to the 1D test case, using a full dynamic procedure with a blending factor $f = 1$ ($ldc.1b_{60\times60}$), still leads to good results, although a slight loss of accuracy can be noticed in high-gradient regions. If the continuity equation is not corrected ($ldc.1c_{60\times60}$), a significant loss of quality is observed, due to the apparently large error on the mass balance. Therefore, from now on we use the exact truncation model for the continuity equation. To examine whether the convective terms are dominant in the modelling of the truncation error, we performed two simulations in which the contributions of the pressure term and the viscous term in the model are neglected. For the first case ($ldc.2a_{60\times60}$) the viscous terms and the pressure terms are not used in the evaluation of the Leonard term. In the second case ($ldc.2b_{60\times60}$), all contributions are maintained, so the complete momentum equations are used in the Leonard term. Thus, in the latter case, we implicitly assume that the model of the convective term can account for the overall error. In other words, we merge the correction for pressure and viscous terms into the convective part. It can be seen from the results of $ldc.2b_{60\times60}$ in Fig. 15 that such an assumption is not justified. Nevertheless, case $ldc.2a_{60\times60}$ leads to good results. This indicates that the convective terms are dominant, and that correction of these terms gives a significant quality improvement. This led us to further investigate Smagorinsky-like approximations for these non-linear terms. Results of such different Smagorinsky-like models are shown in Fig. 16. It can be seen that the first Smagorinsky model, in which the dynamic field is dimensional, yield reasonable results if the contributions of the viscous term and the pressure term are accounted for, whether with

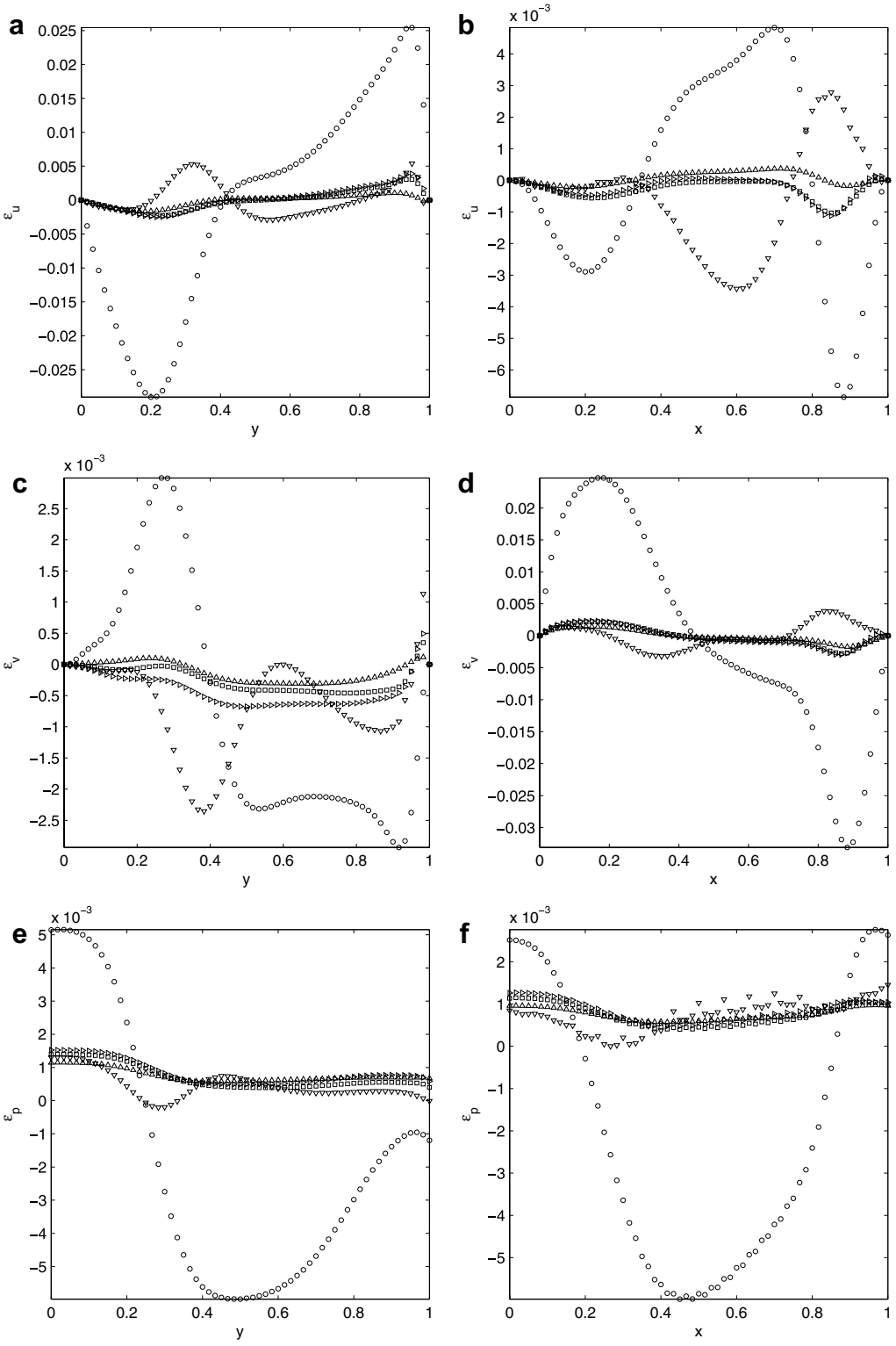

Fig. 13. Error levels: (△) ldc.6o$_{60\times60}$; (□) ldc.4o$_{60\times60}$; (○) ldc.2o$_{60\times60}$; (▽) ldc.RE$_{60\times60}$; (▷) ldc.DRE$_{60\times60}$.

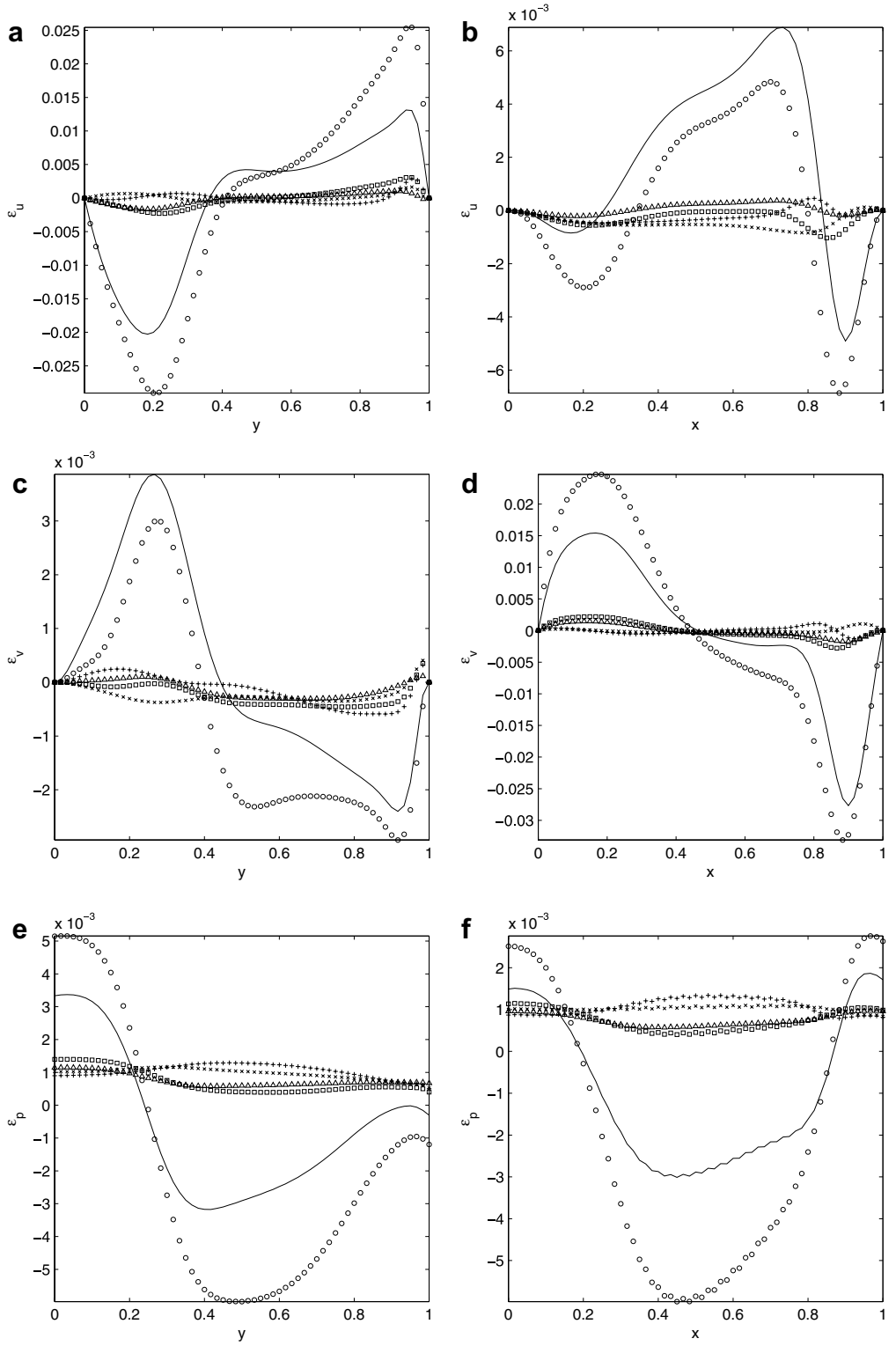

Fig. 14. Error levels: (△) ldc.6o$_{60\times60}$; (□) ldc.4o$_{60\times60}$; (○) ldc.2o$_{60\times60}$; (×) ldc.1a$_{60\times60}$; (+) ldc.1b$_{60\times60}$; (—) ldc.1c$_{60\times60}$.

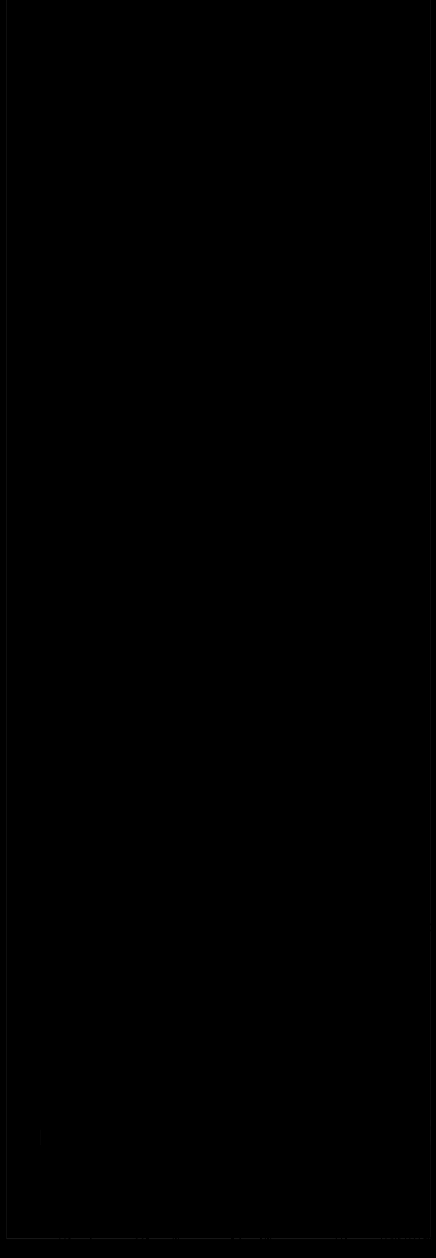

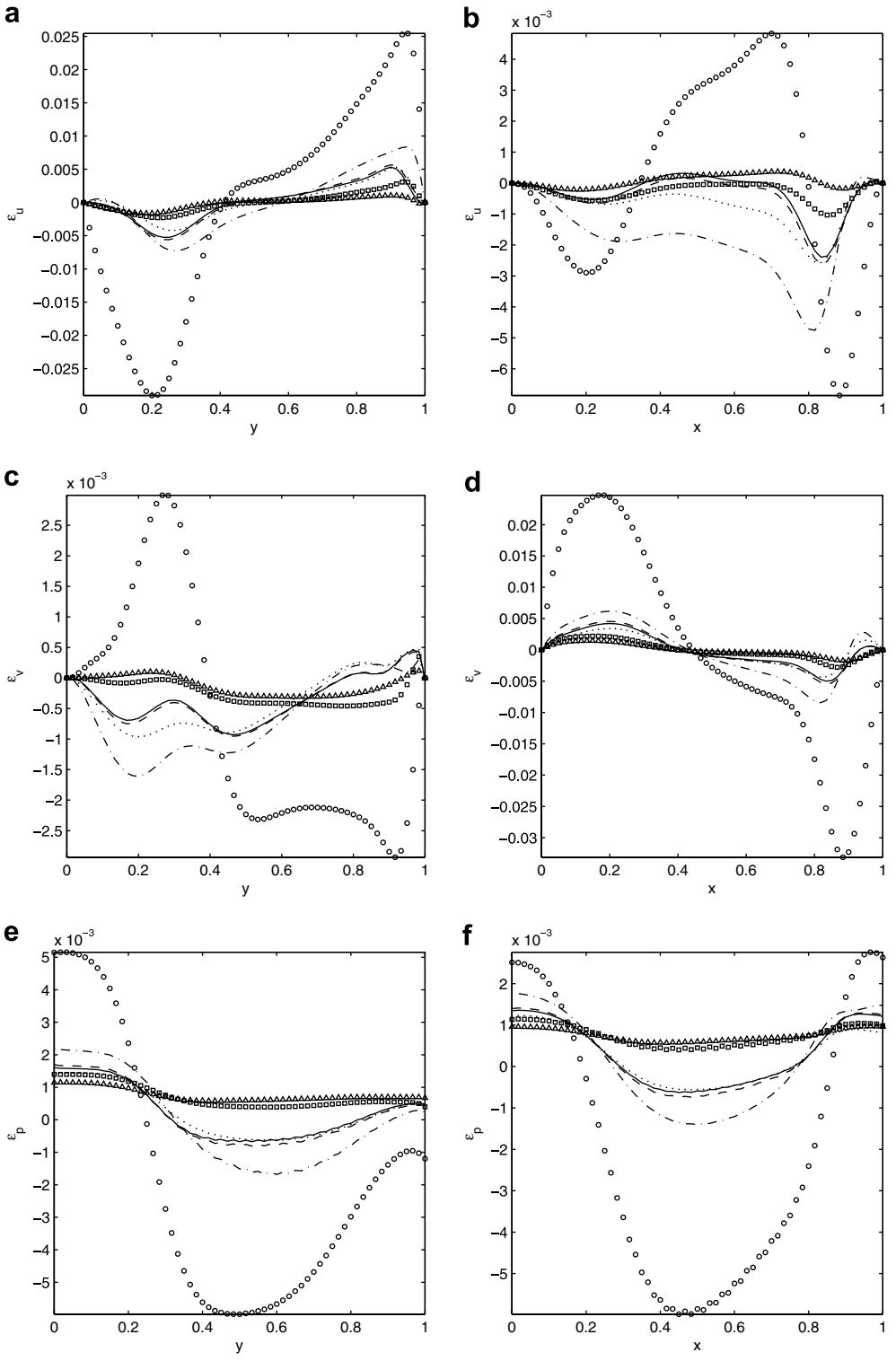

Fig. 16. Error levels: (△) ldc.6o$_{60\times60}$; (□) ldc.4o$_{60\times60}$; (○) ldc.2o$_{60\times60}$; (—) ldc.3a$_{60\times60}$; (---) ldc.3b$_{60\times60}$; (-·-) ldc.3c$_{60\times60}$; (···) ldc.3d$_{60\times60}$.

an exact dynamic procedure, or an exact fourth-order implementation. However, if only the Smagorinsky model is used without a model for pressure and viscous terms, the results become less accurate. Taking the second Smagorinsky-like model, in which the non-dimensional field is obtained dynamically, results are again good, even without correction for the pressure terms and the viscous terms. This points out that it is not fully justified for the procedure to obtain a dimensional dynamic field, probably because this field cannot be assumed as grid independent.

To complete this work, a final grid-refinement study on the error norms was done, using the grid resolutions 120×120,90×90,60×60 and 30×30. Results are shown in Fig. 17. First it can be seen from the L_1-norm, which is the most natural error norm, that although we implemented up to a sixth-order accurate scheme, results only display at maximum a slope of 4, the sixth-order scheme included. The reason behind this somewhat masked result is most likely the implementation of the boundary conditions of the pressure field. The fourth-order accurate Neumann condition $\frac{\partial^3 p}{\partial n^3} = 0$ for the pressure field causes that the pressure field cannot exceed fourth order at the walls of the cavity where the pressure gradients are very large. This makes for instance that the $L_{\infty p}$ remains approximately constant in the grid spacing. The maximum error of the pressure field is situated in the corner singularity at the wall of the cavity. Consequently it is obvious that also the velocity components are affected by this restriction, such that the corresponding error norms does not display a sixth-order slope. Nevertheless the error is still smaller than that of the fourth-order scheme. These observations make it rather difficult to judge correctly the grid-refinement study. From the L_1-velocity norms it seems that the dynamic procedure combined with the exact model obtains higher accuracy than the fourth-order solution, even as good as the sixth-order solution, but only for the coarser grids up to 60×60. However, for the finer grids, one can observe again a deflection making the accuracy somewhat lower than the fourth-order solution. This trend is not seen in the L_2-velocity norms, where the lowest accuracy of the procedure is still that of the fourth-order solution. Also from the L_1 and L_2 pressure norms it clearly seems that the procedure has the same performance as the fourth- and sixth-order schemes. The reason for the slope-deflection should again be found in the approximations made in the model. We assumed in the exact truncation model, that all dynamic coefficients of each derivative could be merged into one dynamic coefficient for

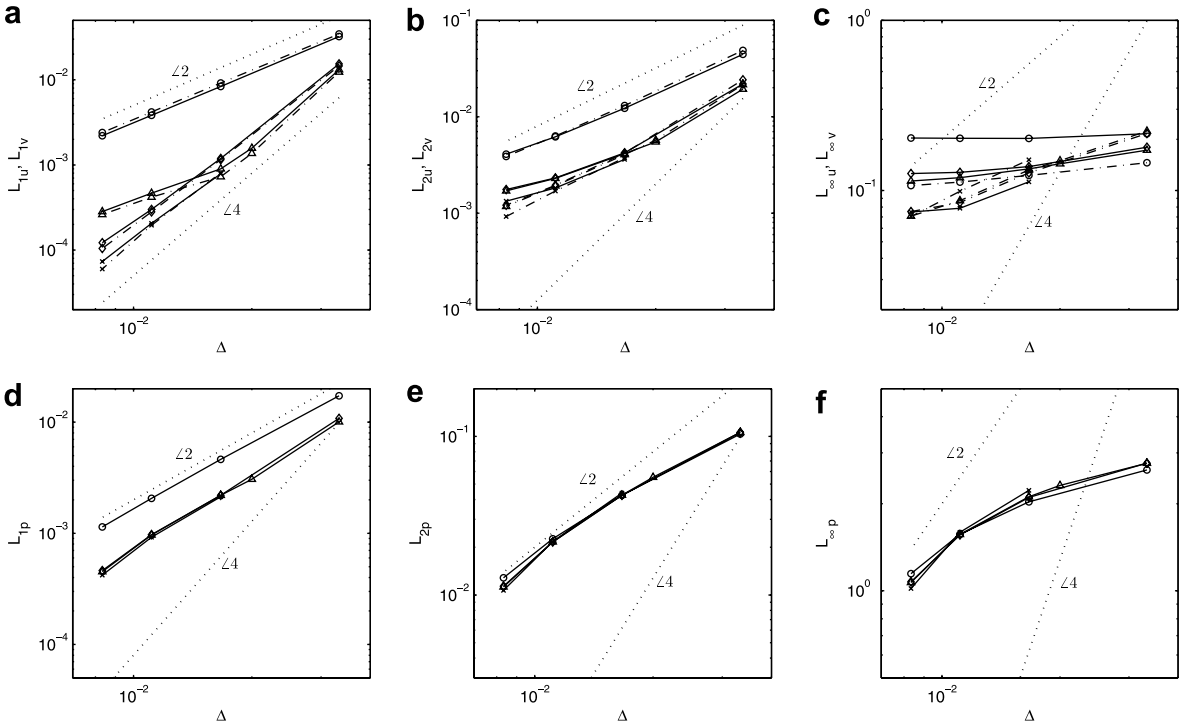

Fig. 17. Error norms L_1, L_2 and L_∞ for the second order (○), fourth order (◇), sixth order (×) solutions and the dynamic procedure with $f = \frac{1}{5}$ (△): a, b, c give the errornorms for u-velocity (–) and v-velocity (-·-); d, e, f give the error norms for the pressure field.

each equation, which is optimized by the procedure using least-squares. Of course, for the finer grids corrections are more subtile than for coarse grids, making it more difficult for the procedure to find one optimal common least-square coefficient. The best the procedure can do is then approximately fourth-order accuracy. For the coarse grids however, the procedure can make a difference by finding one optimal common least-square coefficient, because the relative importance of a high-order correction in the coefficient becomes larger with the grid spacing. It is obvious that the more approximations one makes in the modelling or in the procedure, the less gain in accuracy can be obtained.

6. Conclusions

Discretization errors in numerical simulations should be small in order to provide sufficient accuracy. Complexity of high-order schemes, or the computational cost of fine meshes (in combination with low-order schemes) are often prohibitive in computational fluid dynamics. In this work, we presented the sampling-based dynamic procedure as a tool to enhance numerical accuracy, which is a compromise between stencil-complexity and computational cost. The proposed technique uses two different grid resolutions to estimate and correct the truncation error. After introducing the general theory, the relationship of the dynamic procedure with Richardson extrapolation was shown. Moreover, a spectral analysis of the dynamic procedure for both a single wave and a double wave shows its capability of increasing the accuracy of a finite difference discretization with several orders. Application of this technique to a 1D convection–diffusion equation and a square-driven cavity demonstrates the potential, and confirms the theoretical findings. In the following we summarize the main conclusions obtained in the present research.

(i) The sampling-based dynamic procedure can be used as a technique to improve the numerical quality of a discretization scheme. The dynamic procedure applied to a second-order central discretization of a derivative results in a sixth-order accurate scheme for a blending factor of $f = \frac{1}{5}$. Varying this blending factor allows one to optimize the scheme for higher accuracy of certain intervals in the wavenumber range. The complexity of implementing the stencils is limited to that of a fourth-order discretization. The method may be particularly interesting in the context of multilevel algorithms because it is based on discretizations on multiple grid resolutions. Therefore, it may be a natural supplement of multigrid-like methods, with minimal additional computational cost.

(ii) The dynamic procedure applied to a second-order central discretization of a complete partial differential equation in combination with an exact truncation error model, results in a significant gain in accuracy, at least better than a fourth-order scheme. The procedure then acts like an optimization procedure by minimizing the local truncation error. The procedure is liable to certain assumptions or simplifications made in the procedure and/or the truncation error model. This leads to a small loss in quality, for instance the slope of grid-convergence is not fully maintained. These observations seem to be relatively more important for fine grids, whereas for coarse grids the optimization has a more pronounced and positive effect.

(iii) It was shown that both the classical and differential Richardson extrapolations are special formulations of the technique, with an additional approximation. Results of the classical form where found to be disappointing compared to those of its differential counterpart. The differential Richardson extrapolation obtains fourth-order accuracy, whereas the classical Richardson extrapolation does not get to fourth-order accuracy.

(iv) A severe loss of quality is observed if the truncation error of the continuity equation is not corrected. Moreover, it is observed that the truncation errors of the convective terms in the momentum equations are dominant, and accounting for these terms only, leads to good results.

(v) Using a modelling hypothesis, the higher-order derivatives in the truncation errors of the convective terms in the momentum equations were reduced to a product of lower-order derivatives, resulting in a Smagorinsky-like models for these terms. Consequently, one avoids the complexity of evaluating high-order derivatives. The dynamic procedure, in combination with a Smagorinsky-like model for the truncation error of the convective terms still leads to a significant accuracy improvement. However, lower quality compared to the use of the exact truncation error model was observed, as no full fourth order could be reached. Still, results are remarkably better than second-order solution.

Acknowledgement

This research was funded by a Ph.D. grant of the Institute for the Promotion of Innovation through Science and Technology in Flanders (IWT-Vlaanderen).

References

[1] S. Ghosal, J. Comput. Phys. 125 (1996) 187.
[2] A.G. Kravchenko, P. Moin, J. Comput. Phys. 131 (1997) 310.
[3] F.K. Chow, P. Moin, J. Comput. Phys. 184 (2003) 366.
[4] G. Winckelmans, L. Georges, L. Bricteux, H. Jeanmart, in: 57th Annual Meeting of the American Physical Society Division of Fluid Dynamics, Seattle, November 2004, Bull. Am. Phys. Soc. Div. Fluid Dyn. 49 (2004).
[5] G. Winckelmans, L. Bricteux, L. Georges, G. Daeninck, H. Jeanmart, The sampling-based dynamic procedure for LES: investigations using finite differences, in: E. Lamballais, R. Friederich, B. Geurts, O. Métais (Eds.), Ercoftac Series – Direct and Large-Eddy Simulations, 6, Ercoftac, Springer, Poitiers, 2005, pp. 183–190.
[6] O. Debliquy, B. Knaepen, D. Carati, A.A. Wray, Sampling versus filtering in large-eddy simulations, in: P. Moin, N.N. Mansour (Eds.), Proceedings of the Summer Program 2004, Stanford University and Nasa Ames Research Center, Stanford, 2004, pp. 133–144.
[7] B. Knaepen, O. Debliquy, D. Carati, J. Comput. Phys. 205 (2005) 98.
[8] M. Germano, U. Piomelli, P. Moin, W.H. Cabot, Phys. Fluids A 3 (1991) 1760.
[9] H. Jeanmart, G. Winckelmans, Comparison of recent dynamic subgrid-scale models in turbulent channel flow, in: P. Bradshaw (Ed.), Proceedings of the Summer Program 2002, Stanford University and Nasa Ames Research Center, Stanford, 2002, pp. 105–116.
[10] W. Shyy, M. Garbey, A. Appukuttan, J. Wu, Numer. Heat Transfer, Part B 41 (2002) 139.
[11] R. Verstappen, A. Veldman, J. Eng. Math. 32 (1997) 143.
[12] R. Verstappen, A. Veldman, J. Comput. Phys. 187 (2003) 343.
[13] P. Roache, AIAA J. 36 (1998) 696.